Alexandria Engineering Journal 113 (2025) 60–73

Contents lists available at ScienceDirect

Alexandria Engineering Journal

journal homepage: www.elsevier.com/locate/aej

Original article

Fractional-order PID feedback synthesis controller including some external influences on insulin and glucose monitoring

Kottakkaran Sooppy Nisar [a,*], Muhammad Farman [b,c], Khadija Jamil [d], Saba Jamil [d], Evren Hincal [b]

[a] Department of Mathematics, College of Science and Humanities in Alkharj, Prince Sattam Bin Abdulaziz University, Alkharj 11942, Saudi Arabia
[b] Faculty of Arts and Sciences, Department of Mathematics, Near East University, Northern Cyprus, Turkey
[c] Department of Computer Science and Mathematics, Lebanese American University, 1102-2801, Beirut, Lebanon
[d] Institute of Mathematics, Khwaja Fareed University of Engineering and Information Technology, Rahim Yar Khan, Pakistan

ARTICLE INFO

Keywords:
Beta-cells
Complex diabetes model
Hyperglycemia
Ulam–Hyers stability
PID
Controllability
Mittag-Leffler kernel

ABSTRACT

The article aims to develop a fractional-order proportional integral derivative (PID) controller to monitor insulin and glucose levels in humans under the influences of stress, excitement, and trauma. A novel fractional-order diabetes mellitus model is proposed, incorporating a nonsingular, nonlocal kernel (Mittag-Leffler function) to account for the effect of epinephrine on suppressing insulin secretion and the dynamics of beta-cell mass. As beta-cell mass increases in the presence of adrenaline, the system remains highly responsive to rising blood glucose and falling insulin levels, driven by the hormone's suppressive effects. The key advantage of this model is its ability to incorporate these physiological stressors and use fractional-order derivatives to describe the nonlocal dynamics within the system. The innovations of this work include a fractional-order diabetes mellitus model that captures the biological memory and hereditary effects of glucose regulation under stress, and a fractional-order PID controller that offers greater stability and robustness compared to conventional controllers, particularly in managing adrenaline-induced hyperglycemia. The model's positivity, boundedness, and equilibrium solutions are rigorously analyzed to ensure feasibility. Additionally, a new theorem is proven using fixed-point theory, confirming the existence and uniqueness of the fractional-order model. Ulam–Hyers stability analysis further demonstrates the model's robustness and well-posedness, while qualitative properties are explored. Numerical simulations to explore which is done by solutions with a two-step Lagrange polynomial for generalized Mittag Leffler kernel showed that prolonged and severe hyperglycemia was caused by regular release of adrenaline into the blood at different fractional order values and fractal dimensions by changing initial values for normal and diabetes patients. PID and controller results are analyzed to increase the stability of the system to monitor and assess of glucose–insulin system with beta cell mass to control the hyperglycemia. Lastly, the results are obtained and visually shown using graphical representations, which provide empirical evidence in support of our theoretical findings. At the end comparison of numerical simulations is constructed to show the efficiency, convergence, and accuracy of proposed techniques at different fractional values with power law and exponential kernels. Numerical simulations, mathematical modeling, and analysis work together to shed light on the dynamics of diabetes mellitus and make important advances in the knowledge and treatment of this common disease.

1. Introduction

The metabolic condition known as diabetes mellitus is typified by abnormally elevated blood and urine sugar levels. The body cannot metabolize all of the sugars because there is not enough insulin in the body. The control of blood sugar levels is among the human body's most intricately regulated systems. The bloodstream's delicate balance between glucose and insulin levels is typically maintained [1]. A disorder of the glucose regulation system characterized by high blood sugar levels during fasting and/or after meals is another way to describe diabetes mellitus [2]. There are two forms of diabetes, according to [3]: Type 1 diabetes Type 2 diabetes. High levels of blood sugar, known as hyperglycemia, are a result of diabetes mellitus. Diabetes mellitus is a disorder of metabolism that is usually caused by a mix of genetic and environmental factors [4]. Two negative feedback loops control

* Corresponding author.
E-mail address: n.sooppy@psau.edu.sa (K.S. Nisar).

https://doi.org/10.1016/j.aej.2024.11.017
Received 16 July 2024; Received in revised form 6 October 2024; Accepted 4 November 2024
Available online 16 November 2024

the amount of blood glucose. Short-term hyperglycemia causes the pancreatic β-cells to release insulin more quickly. The increase in blood insulin levels causes a reduction in the liver's production of glucose and a boost in the uptake of glucose. This leads to a decrease in blood glucose levels [1]. According to recent research, persistent hyperglycemia may be involved in a second negative feedback loop by altering the rates of β-cell death and replication, which would increase the mass of β-cells that secrete insulin [3]. A larger quantity of β-cells indicates a greater ability to secrete insulin, which would lower blood glucose levels. Defects in elements of the chronic and short-term negative feedback loops have been linked to type 2 diabetes. Insulin resistance, insulin secretory abnormalities, and insufficient β-cell mass are all linked to type 2 diabetes; however, these flaws are also present in non-diabetic individuals. Patients with type 2 diabetes have 50% to 100% lower insulin-stimulated glucose disposal than non-diabetic controls. However, comparable levels of insulin resistance have also been reported in a number of non-diabetic participants, including obese adults, as well as during pregnancy, puberty, and old age [3].

Atangana [5] has introduced the fractal–fractional derivative, a completely new method for fractional calculus. The concept underlying this topic is often highly beneficial for resolving certain challenging problems. The operator has two orders: fractional order and fractal dimension. This innovative approach to fractal fractions outperforms the standard way [6,7]. This is so that when working with fractal–fractional derivatives, one can concurrently study fraction operators and fractal dimensions. This operator's primary benefit is in its ability to build models that more accurately represent systems that exhibit memory effects. In contrast to conventional integer-order models, fractional-order epidemic models [8] provide a more accurate depiction of disease dynamics by accounting for regional heterogeneity and long-term memory effects. The information dynamics of the human brain, especially sensory memory are modeled by fractional-order deterministic mathematical models in [9]. In this work we include fractional-order derivatives to try and model information-processing behavior in the brain more accurately. Article [10] introduces a mathematical model involving fractional order with non-singular kernel Mittag-Leffler law for COVID-19 pandemic. This leads to formulate the dynamics of illness in a more realistic fashion as compared with integer-order models that is only likely and possible using fractal calculus-based differential processes. To investigate dynamical transmission with eight compartments the authors [11] suggest a nonlinear fraction order Ebola virus model based on an original piecewise hybrid method. This paper [12] offers a comprehensive fractional-order modeling and analysis platform for the dynamics of MRSA bacterial infection by leveraging the elasticity inherent in fractional calculus. This frame work makes it possible to grasp the complex behavior of a system more effectively. A novel concept of fractal–fractional (FF) derivatives was introduced by Atangana [13] and has been widely used in addressing challenging problems for numerous applications. The FF derivative was used by Farman and colleagues to study plant infection dynamics. [14]. Two-phase Lagrange Picard integration results within the Mittag Leffler kernel framework A plant virus model with time fractional-order dynamics and disease consequences was simulated using this format. The FO mathematical model, which includes type 1 diabetes and normoglycemia, is examined in [15]. To comprehend HIV/AIDS mechanisms, the economic fractional derivative technique was examined [16]. This paper looks at how HIV/AIDS affects FO using an enlarged Mittag-Leffler kernel with a two-step Lagrange polynomial. Sadri et al. [17] introduced an operational technique using collocation for the KdV–Burgers–Kuramoto problem with variable-order time–space fractions. For the exploration of computational solutions, they utilized a linear array of two-dimensional Jacobi polynomials as the basis functions. Farman et al. [18] proposed a model of non-integer fractal–fractional Mittag-Leffler operator for cancer treatment. The study proposes analytical solutions that are obtained from fractional diffusion equations. These solutions are necessary for the study of the space–time distribution of tumor growth under different conditions: impact of treatment or the presence of intrinsic cell mutations [19]. In co-infection dynamics, the research [20] adds knowledge and justifies the need for a total immunization campaign to reduce the burden of viral diseases on the health of the public. This work has involved the analysis of a mathematical model regarding co-infection of diabetes and TB with emphasis on the relationship and progression of the diseases [21]. As for fractional SEIR models the idea of fractional calculus in general has shown that these models can offer improved functionality of simulation of the actual data than the integer-order models highlighting the important details in disease transmission [22]. Consequently the existence and uniqueness of solutions of partial neutral functional fractional differential equations using fixed point theory with the help of Banach contraction principle and Schauder fixed point theorem under Lipschitz continuity and boundedness of coefficients are demonstrated [23]. This paper [24], considers the issue of the control of nonlinear fractional multi-agent systems, using signed graph to deal with problems caused by input delays, disturbances and switching of network. The study [25], focuses on the problems of consensus in fractional-order multi-agent systems with distributed delays and DoS attacks, offering an efficient defense scheme to improve the system stability and security when operating in complex environments. The work [26], concentrates on constructing anti-disturbance consensus strategy for fractional-order multi-agent systems with time delay based on the Riemann–Liouville fractional derivative. The paper [27], proposed and analyzed a centralized event-triggered control strategy for enhancing the stability of CVPS in the presence of disturbances and artificial time-delay in the coordination and communication of the connected vehicles in a wireless networked environment.

This work proposes a novel approach that incorporates fractal–fractional derivative with Mittag-Leffler kernel for disease dynamics analysis. The reason for using the fractional-order model as opposed to a conventional integer-order model was based on its capability to effectively capture the memory, hereditary, and nonlocality of various diabetes mellitus insulin–glucose dynamics. This results in more realistic and accurate modeling, higher predictive accuracy of long-term prognosis, and more stability and control in managing diabetes thus making this approach superior for modeling a complex chronic disease such as diabetes. Since Mittag-Leffler function can generalize exponential decay, include memory and nonlocal influence, and exclude singularity, it is used as the kernel in the fractional-order model. These features make it convenient for modeling numerous and repeatedly changing interactions between insulin and glucose in the case of diabetes, which makes it possible to provide a more realistic behavior of the disease and therefore to increase the efficiency of stabilization methods. The document is structured as follows: Section 1 Introduction: Provides a summary of the study goals and objectives.

Section 2 Fundamental Definitions: Offers definitions of the operator used in the analysis.

Section 3 Fractal–Fractional Order Mathematical Model: Introduces a mathematical model that incorporates both fractal and fractional concepts along with the Mittag-Leffler kernel for studying the diabetes model.

Section 4 Analysis of the Proposed Model: Conducts an in-depth analysis of the suggested model.

Section 5 Ulam–Hyers Stability Examination: Examines the stability of the proposed model using Ulam–Hyers stability criteria.

Section 6 PID and Controllability Examined.

Section 7 Numerical Findings: Presents numerical results obtained from applying the model.

Section 8 Results and Discussion: Combines results and detailed discussions.

Section 9 Conclusion: Summarizes all findings and presents a conclusion.

2. Basic concepts

Here, we offer a few of crucial definitions that could make system analysis easier.

Definition 2.1 ([13,28,29]). Assume that $\mathscr{T}(t)$ is fractal-differentiable with order ς and continuous in the interval (a,b). The fractal–fractional derivative of order ς can then be stated in terms of the Riemann–Liouville derivative for $0 \le \varsigma, \upsilon \le 1$.

- for power law:

$$ {}_0^{FFP}\mathrm{D}_t^{\varsigma,\chi}\,\mathscr{T}(t) = \frac{1}{\Gamma(n-\varsigma)}\frac{d}{dt^{\chi}}\int_0^t (t-\wp)^{n-\varsigma-1}\,\mathscr{T}(\wp)d\wp. \tag{1}$$

  where $n-1 < \varsigma, \chi < n \in \mathscr{N}$. And $\frac{\mathrm{D}\mathscr{T}(\wp)}{\mathrm{D}\wp^{\chi}} = \lim_{t\to\varphi}\frac{\mathscr{T}(t)-\mathscr{T}(\wp)}{t^{\chi}-\wp^{\chi}}$

- for exponential:

$$ {}_0^{FFE}\mathrm{D}_t^{\varsigma,\chi}\,\mathscr{T}(t) = \frac{\mathfrak{S}(\varsigma)}{\Gamma(n-\varsigma)}\frac{d}{dt^{\chi}}\int_0^t \exp\Big[-\frac{\varsigma}{1-\varsigma}(t-\wp)\Big]\mathscr{T}(\wp)d\wp \tag{2}$$

  where $\varsigma > 0, \chi \le n \in \mathscr{N}$, and $\mathfrak{S}(0) = 1 = \mathfrak{S}(1)$.

- for Mittag-Leffler:

$$ {}_0^{FFM}\mathrm{D}_t^{\varsigma,\chi}\,\mathscr{T}(t) = \frac{\mathscr{AB}(\varsigma)}{1-\varsigma}\frac{d}{dt^{\chi}}\int_0^t \mathscr{T}(\wp)\mathscr{E}_{\varsigma}\Big[-\frac{\varsigma}{1-\varsigma}(t-\wp)^{\varsigma}\Big]d\wp. \tag{3}$$

  where $0 < \varsigma, \chi \le 1$, $\mathscr{E}_{\varsigma}$ is the Mittag Leffler function and $\mathscr{AB}(\varsigma) = 1-\varsigma+\frac{\varsigma}{\Gamma(\varsigma)}$ indicates a function of normalization.

Definition 2.2 ([13,28,29]). If $\mathscr{T}(t)$ is continuous on (a,b) and $0 \le \varsigma, \vartheta \le 1$ then $\mathscr{T}(t)$ has a fractional order of ς and a fractal dimension of χ.

- for power law:

$$ {}_0^{FFP}\mathrm{I}^{\varsigma,\chi}\,\mathscr{T}(t) = \frac{1}{\Gamma(\varsigma)}\int_0^t (t-\wp)^{\varsigma-1}\wp^{1-\chi}\,\mathscr{T}(\wp)d\wp. \tag{4}$$

- for exponential:

$$ {}_0^{FFE}\mathrm{I}^{\varsigma,\chi}\,\mathscr{T}(t) = \frac{\chi(1-\varsigma)t^{\chi-1}\mathscr{T}(t)}{\mathfrak{S}(\varsigma)} + \frac{\varsigma\chi}{\mathfrak{S}(\varsigma)}\int_0^t \wp^{\varsigma-1}\,\mathscr{T}(\wp)d\wp. \tag{5}$$

- for Mittag-Leffler:

$$ {}_0^{FFM}\mathrm{I}^{\varsigma,\chi}\,\mathscr{T}(t) = \frac{\chi(1-\varsigma)t^{\chi-1}\mathscr{T}(t)}{\mathscr{AB}(\varsigma)} + \frac{\varsigma\chi}{\mathscr{AB}(\varsigma)\Gamma(\varsigma)}\int_0^t (t-\wp)^{\varsigma-1}\wp^{\chi-1}\,\mathscr{T}(\wp)d\wp. \tag{6}$$

Definition 2.3 ([30]). Let $a,b \in \mathbb{R}$, $a < b\,[a,b] \subset \mathbb{R}$. The space of continuous function from the subset $[a,b]$ to $\mathbb{R}$ is defined by

$$C([a,b],\mathbb{R}) = \{f : [a,b] \to \mathbb{R}, f \in C[a,b]\}$$

with the norm

$$\|f(x)\|\,C([a,b]) = \max_{x\in[a,b]}|f(x)|. \tag{7}$$

Definition 2.4 ([30]). Let $a,b \in \mathbb{R}$, $a < b$. We denote by $C^1([a,b])$ the space of real-valued function $f(x)$ whose derivative f' is continuous on $[a,b]$ with norm

$$\|f(x)\|\,C^1([a,b]) = \max_{x\in[a,b]}|f(x)| + \max_{x\in[a,b]}|f'(x)|. \tag{8}$$

3. Model formulation

The model was analyzed in [31], here G refers to glucose, I to insulin and β is incorporated for the dynamics of the beta cells. Stress, excitement and trauma are types of factors that can change the homeostatic balance of glucose and insulin according the model. In this paper, we have given the fractal–fractional operator for continuous time in Atangana–Baleanu's sense which is effective for modeling of real life systems and phenomenon and further helps us in understanding epidemic dynamics and disease transmission. The fact that it could represent both fractional-order dynamics and fractal process makes this method suitable for investigating the real-world problems. The suggested fractional order PID controller is very efficient in regulating insulin–glucose dynamics during stress, excitement or trauma, when adrenaline produces hyperglycemia due to alteration in the normal insulin secretion. It is in harmony with the steady changes of the body and better for controlling blood sugar levels during exercise or acute illness than with an ordinary stick-shaped controller. The present controller contributes to keeping the blood glucose levels in check to avoid any risky fluctuations in these conditions.

Table 1
Model parameters.

Symbol	Description [31]	Value
R_0	No glucose production occurs	864
E_{GO}	Complete glucose efficiency at zero insulin	1.14
S_I	Complete sensitivity to insulin	0.72
σ	Maximum amount of insulin released	43.2
α	Point at which the sigmoidal function inverts	20,000
K	Rate at which muscles, liver, and kidneys remove insulin	432
d_0	Rate of spontaneous demise of beta cells	0.06
r_1, r_2	Constant ranges of beta cell glucose tolerance	$0.00084, 0.24\times10^{-5}$
ρ	The ability of epinephrine to inhibit insulin secretion	140
G_e	Increase in glucose because to adrenaline release	41%

The new fractional model is given by the following system of nonlinear fractal–fractional differential equations, respect to the Atangana–Baleanu sense for $0 < \varsigma, \chi \le 1$:

$$\begin{cases} {}^{FFM}D_{0,t}^{\varsigma,\chi}G(t) = R_0 + G_e - \left(E_{GO} - S_I I\right)G, \\ {}^{FFM}D_{0,t}^{\varsigma,\chi}I(t) = \frac{\beta\sigma G^2}{(\alpha+G^2)} - (\rho - K)I, \\ {}^{FFM}D_{0,t}^{\varsigma,\chi}\beta(t) = \left(-d_0 + r_1 G + r_2 G^2\right)\beta, \end{cases} \tag{9}$$

with the initial conditions

$$G(0) \ge 0\,, \quad I(0) \ge 0\,, \quad \beta(0) \ge 0.$$

Table 1 also shows the settings of the parameters used in the fractional-order diabetes model and the fractional-order PID controller that determines the accurate glucose–insulin dynamics especially in stress, excitement and trauma. These values are related to basic physiological characteristics regarding to glucose–insulin interaction including insulin secretion rates σ, stress hormone influences over insulin inhibition ρ. In Table 1, K is the insulin clearance constant by liver, kidney, muscle and insulin receptor R_0 is the net rate of glucose production and at zero glucose level G_0 is the amount of glucose increase due to epinephrine hormones E_{GO} total glucose effectiveness at zero insulin for production and utilization and S_I is the total insulin effective. relevant sensitivity in production and utilization for its effectiveness. To make these values realistic and realistic, the required values were taken from validated clinical data, physiological databases and literature on diabetes and endocrinology. The interaction between epinephrine, beta-cell mass, and insulin secretion was derived to mimic the chronic implications of stress on glucose homeostasis. Including these dynamics into the fractional-order model, the paper illustrates how the proposed controller addresses stress-induced hyperglycemia challenges for more stable and appropriate glucose–insulin regulation.

3.1. Positive bounded solutions

As the processes of the proposed model are bounded and positive with certainty, we investigate under which conditions it can be applied

to important real-world scenarios. For every $\forall t \geq 0$, we have the following information in terms of classical derivatives:

$$I(t) \geq I(0)\, e^{(\rho-K)t}.$$

To determine the norm, we must: $\|\mathscr{P}\|_\infty = \sup_{t\in D_{\mathscr{P}}} |\mathscr{P}(t)|$. After that, we find

$$\begin{aligned} {}^{FFM}D_{0,t}^{\varsigma,\chi} G(t) &= R_0 + G_e - \left(E_{GO} - S_I I(t)\right) G(t) \\ &\geq \left(E_{GO} - S_I I(t)\right) G(t) \\ &\geq \left(E_{GO} - S_I |I(t)|\right) G(t) \\ &\geq \left(E_{GO} - S_I \sup_{t\in I} |I(t)|\right) G(t) \\ &= \left(E_{GO} - S_I |I(t)|_\infty\right) G(t). \end{aligned} \tag{10}$$

then

$$G(t) \geq G(0)\, e^{(E_{GO} - S_I |I(t)|_\infty)t}, \quad \forall t \geq 0.$$

$$\begin{aligned} {}^{FFM}D_{0,t}^{\varsigma,\chi} \beta(t) &= \left(-d_0 + r_1 G(t) + r_2 G^2(t)\right) \beta(t) \\ &\geq \left(-d_0 + r_1 G(t) + r_2 G^2(t)\right) \beta(t) \\ &\geq \left(-d_0 + r_1 |G(t)| + r_2 \left|G^2(t)\right|\right) \beta(t) \\ &\geq \left(-d_0 + r_1 \sup_{t\in G} |G(t)| + r_2 \sup_{t\in G} \left|G^2(t)\right|\right) \beta(t) \\ &= \left(-d_0 + r_1 |G(t)|_\infty + r_2 \left|G^2(t)\right|_\infty\right) \beta(t). \end{aligned} \tag{11}$$

then

$$\beta(t) \geq \beta(0)\, e^{\left(-d_0 + r_1 |G(t)|_\infty + r_2 \left|G^2(t)\right|_\infty\right)t}, \quad \forall t \geq 0.$$

system (9) solutions are consistently positive $\forall t \geq 0$, as stated in [29].

$$\begin{cases} G(t) \geq G(0)\, \Xi_\varsigma \left[-\frac{\psi^{1-\chi}\varsigma\left(E_{GO} - S_I |I(t)|_\infty\right)t^\varsigma}{AB(\varsigma)-(1-\varsigma)\left(E_{GO} - S_I |I(t)|_\infty\right)}\right], \\ I(t) \geq I(0)\, \Xi_\varsigma \left[-\frac{\psi^{1-\chi}\varsigma(\rho-K)t^\varsigma}{AB(\varsigma)-(1-\varsigma)(\rho-K)}\right], \\ \beta(t) \geq \beta(0)\, \Xi_\varsigma \left[-\frac{\psi^{1-\chi}\varsigma\left(-d_0 + r_1 |G(t)|_\infty + r_2 \left|G^2(t)\right|_\infty\right)t^\varsigma}{AB(\varsigma)-(1-\varsigma)\left(-d_0 + r_1 |G(t)|_\infty + r_2 \left|G^2(t)\right|_\infty\right)}\right]. \end{cases}$$

3.2. Equilibrium points

The following are the equilibrium states of the suggested model (9):

$$E^\bullet = (G^\bullet, I^\bullet, \beta^\bullet) = \left(\frac{R_0 + G_e}{E_{GO}}, 0, 0\right)$$

4. Existence and uniqueness result

The main goal of analysis is to use fixed point theorems to show that nonlinear systems have solutions. Fixed-point contractions are used in nonlinear functional analysis to demonstrate the presence of solutions in particular systems. In Banach spaces, fixed point mappings make it easier to achieve complete comprehension. Find out if a solution exists and if it is unique. There will only be one solution for the model given in Eq. (9) in $[0, \mathbb{T}]$, according to a fixed point mappings theorem. Taking into account Eq. (9), we can understand it as

$$\begin{cases} {}^{FFM}D_{0,t}^{\varsigma,\chi} G(t) = R_0 + G_e - \left(E_{GO} - S_I I\right) G, \\ {}^{FFM}D_{0,t}^{\varsigma,\chi} I(t) = \frac{\beta\sigma G^2}{(\alpha+G^2)} - (\rho - K) I, \\ {}^{FFM}D_{0,t}^{\varsigma,\chi} \beta(t) = \left(-d_0 + r_1 G + r_2 G^2\right) \beta, \end{cases} \tag{12}$$

The Mittag Leffler kernel (9) is utilized to recast Eq. (12) as a Fractal–Fractional integral.

$$\begin{aligned} G(t) &= G(0) + \frac{\chi(1-\varsigma)t^{\chi-1}}{\mathscr{A}\mathscr{B}(\varsigma)} \bar{G}(t, G(t)) \\ &\quad + \frac{\varsigma\chi}{\mathscr{A}\mathscr{B}(\varsigma)\Gamma(\varsigma)} \int_0^t (t-\wp)^{\varsigma-1} \wp^{\chi-1} \bar{G}(\wp, G(\wp)) d\wp = X_1 + X_2, \\ I(t) &= I(0) + \frac{\chi(1-\varsigma)t^{\chi-1}}{\mathscr{A}\mathscr{B}(\varsigma)} \bar{I}(t, I(t)) \\ &\quad + \frac{\varsigma\chi}{\mathscr{A}\mathscr{B}(\varsigma)\Gamma(\varsigma)} \int_0^t (t-\wp)^{\varsigma-1} \wp^{\chi-1} \bar{I}(\wp, E(\wp)) d\wp = Y_1 + Y_2, \\ \beta(t) &= \beta(0) + \frac{\chi(1-\varsigma)t^{\chi-1}}{\mathscr{A}\mathscr{B}(\varsigma)} \bar{\beta}(t, \beta(t)) \\ &\quad + \frac{\varsigma\chi}{\mathscr{A}\mathscr{B}(\varsigma)\Gamma(\varsigma)} \int_0^t (t-\wp)^{\varsigma-1} \wp^{\chi-1} \bar{\beta}(\wp, I(\wp)) d\wp = Z_1 + Z_2, \end{aligned} \tag{13}$$

$$\begin{aligned} X_1 &= G(0) + \frac{\chi(1-\varsigma)t^{\chi-1}}{\mathscr{A}\mathscr{B}(\varsigma)} \bar{G}(t, G(t)), \\ Y_1 &= I(0) + \frac{\chi(1-\varsigma)t^{\chi-1}}{\mathscr{A}\mathscr{B}(\varsigma)} \bar{I}(t, I(t)), \\ Z_1 &= \beta(0) + \frac{\chi(1-\varsigma)t^{\chi-1}}{\mathscr{A}\mathscr{B}(\varsigma)} \bar{\beta}(t, \beta(t)), \end{aligned} \tag{14}$$

$$\begin{aligned} X_2 &= \frac{\varsigma\chi}{\mathscr{A}\mathscr{B}(\varsigma)\Gamma(\varsigma)} \int_0^t (t-\wp)^{\varsigma-1} \wp^{\chi-1} \bar{G}(\wp, G(\wp)) d\wp, \\ Y_2 &= \frac{\varsigma\chi}{\mathscr{A}\mathscr{B}(\varsigma)\Gamma(\varsigma)} \int_0^t (t-\wp)^{\varsigma-1} \wp^{\chi-1} \bar{I}(\wp, I(\wp)) d\wp, \\ Z_2 &= \frac{\varsigma\chi}{\mathscr{A}\mathscr{B}(\varsigma)\Gamma(\varsigma)} \int_0^t (t-\wp)^{\varsigma-1} \wp^{\chi-1} \bar{\beta}(\wp, \beta(\wp)) d\wp, \end{aligned} \tag{15}$$

Using Krasnoselski's fixed point theorem, we demonstrate the fundamental aspect of the governing formulas (12): the expressions $Q(X_1, Y_1, Z_1)$ as maps of contractions and $V(X_2, Y_2, Z_2)$ as continuous compact integral components.

Theorem 4.1. *This non-linear mapping $Q(X_1, Y_1, Z_1) : [0, \mathbf{T}] \to \mathbf{R}_l^3$ given in (14)–(15) ensures that constants meet the Lipschitz contractive condition $\mathscr{W}_X, \mathscr{W}_Y, \mathscr{W}_Z, > 0$*

Proof. Analyze the operator $Q(X_1, Y_1, Z_1) : [0, \mathbf{T}] \to \mathbb{R}_l^3$ within the context of a completely normed space

$$\|(G, I, \beta)\| = \max_{t\in[0,\mathbf{T}]} \left\|G(t) + I(t) + \beta(t)\right\| \tag{16}$$

$G, I, \beta \in [0, \mathbf{T}]$

(i) First, we shall demonstrate that a mapping of contractions is represented by $Q(X_1, Y_1, Z_1)$. For G and $\bar{G}$,

$$\begin{aligned} &\left\|X(G, I, \beta)(t) - X\left(\bar{G}, I, \beta\right)(t)\right\| \\ &= \left\|\left(R_0 + G_e - \left(E_{GO} - S_I I\right) G\right) \right. \\ &\quad \left. - \left(R_0 + G_e - \left(E_{GO} - S_I I\right) \bar{G}\right)\right\| \\ &= \left\|-\left(E_{GO} - S_I I\right)\left(G - \bar{G}\right)\right\| \\ &\leq \left\|\left(E_{GO} - S_I \|I\|\right)\right\| \left\|\left(G - \bar{G}\right)\right\| \\ &\leq \mathscr{W}_X \left\|\left(G - \bar{G}\right)\right\|, \end{aligned} \tag{17}$$

where $\mathscr{W}_X = \left(E_{GO} + S_I \|I\|\right)$. Using this approach, we are able to

$$\begin{aligned} \left\|Y(G, I, \beta)(t) - Y(G, \bar{I}, \beta)(t)\right\| &\leq \mathscr{W}_I \|(I - \bar{I})\|, \\ \left\|Z(G, I, \beta)(t) - Y(G, I, \bar{\beta})(t)\right\| &\leq \mathscr{W}_\beta \|(\beta - \bar{\beta})\|, \end{aligned} \tag{18}$$

where $\mathscr{W}_Y = \|\rho + K\|$, $\mathscr{W}_Z = \left\|d_0 + r_1 \|G\| + r_2 \left\|G^2\right\|\right\|$.

It is evident that for $Q(G, I, \beta)$, the following can be derived.

$$\begin{aligned} &\left\|Q(G, I, \beta)(t) - Q(\bar{G}, \bar{I}, \bar{\beta})(t)\right\| \\ &= \frac{\chi(1-\varsigma)t^{\chi-1}}{\mathscr{A}\mathscr{B}(\varsigma)} \max_{t\in[0,\mathbf{T}]} \left|(G, I, \beta)(t) \right. \\ &\quad \left. - (\bar{G}, \bar{I}, \bar{\beta})(t)\right| \end{aligned}$$

$$\leq \frac{\chi(1-\varsigma)t^{\chi-1}}{\mathscr{A}\mathscr{B}(\varsigma)}\left\|(G,I,\beta)(t)-(\bar{G},\bar{I},\bar{\beta})(t)\right\| \leq \frac{\chi(1-\varsigma)t^{\chi-1}}{\mathscr{A}\mathscr{B}(\varsigma)}\mathscr{W} \tag{19}$$

where

$\mathscr{W} = \max[\mathscr{W}_X, \mathscr{W}_Y, \mathscr{W}_Z] < 1$ holds the Lipschitz constant. This suggests that $Q(X,Y,Z)$ is a non-expansive operator.

(ii) Next, we will show that $V(X_2,Y_2,Z_2)$ is continuously compact.

Bounded operators' absolute modulus X, Y and Z specified in (16)–(17) non-zero positive constants $\lambda_X, \lambda_Y, \lambda_Z, \beth_X, \beth_Y$ *and* $\beth_Z$ fulfilling the following bounded-ness inequalities to demonstrate the operator's compactness

$V(X_2,Y_2,Z_2)$.

$$\begin{aligned} |X(t,G)| &\leq \lambda_X\|G\| + \beth_X,\\ |Y(t,I)| &\leq \lambda_Y\|I\| + \beth_Y,\\ |Z(t,\beta)| &\leq \lambda_Z\|\beta\| + \beth_Z. \end{aligned} \tag{20}$$

Assume that a closed subset of $\mathscr{Z}$ is represented by $\mathfrak{B}$.

$$\mathfrak{B} = \left\{(X,Y,Z)\in\mathbb{Z}/\|\mathbf{X},\mathbf{Y},\mathbf{Z}\|\leq\varpi,\ \varpi>0\right\} \tag{21}$$

For $(X,Y,Z)\in\mathfrak{B}$, we find

$$\begin{aligned} \|X_2(t,G)\| &= \max_{t\in[0,\mathbb{T}]}\left|\frac{\varsigma\chi}{\mathscr{A}\mathscr{B}(\varsigma)\Gamma(\varsigma)}\int_0^t(t-\wp)^{\varsigma-1}\wp^{\chi-1}X(\wp,G(\wp))d\wp\right|\\ &\leq \frac{\Psi^{\varsigma,\chi}}{\mathscr{A}\mathscr{B}(\varsigma)\Gamma(\varsigma)}\int_0^{\Psi}(\Psi-\wp)^{\varsigma-1}\wp^{\chi-1}\left|X(\wp,G(\wp))\right|d\wp\\ &\leq \frac{\Psi^{\varsigma,\chi}}{\mathscr{A}\mathscr{B}(\varsigma)\Gamma(\varsigma)}\lambda_X\varpi + \beth_X \end{aligned} \tag{22}$$

Likewise demonstrated for more elements. Finding the maximum norm continues $\|h(X_2,Y_2,Z_2)\|$ as,

$$\begin{aligned} &\|h(X_2,Y_2,Z_2)\|\\ &\leq\left\{\left[\lambda_X+\lambda_Y+\lambda_Z\right]\varpi+\beth_X+\beth_Y+\beth_Z\right\}=\delta \end{aligned} \tag{23}$$

where a positive constant is denoted by δ. Therefore, $\|h(G,I,\beta)\|\leq\delta \Rightarrow$ h is uniformly bounded operator.

Now, we will show that for $t_x < t_y \in [0,\mathbb{T}]$, h is uniformly continuous. We have for $t_1 < t_2 \in [0,\mathbb{T}]$ for this purpose.

$$\begin{aligned} &|X_2(t_2,G)-X_2(t_1,G)|\\ &= \frac{\varsigma\chi}{\mathscr{A}\mathscr{B}(\varsigma)\Gamma(\varsigma)}\left|\int_0^{t_y}(t-\wp)^{\varsigma-1}\wp^{\chi-1}X(\wp,G(\wp))d\wp\right.\\ &\quad\left.-\int_0^{t_x}(t-\wp)^{\varsigma-1}\wp^{\chi-1}X[\wp,G(\wp)]d\wp\right|\\ &\leq \frac{\varsigma\chi}{\mathscr{A}\mathscr{B}(\varsigma)\Gamma(\varsigma)}\left[\int_0^{t_y}(t-\wp)^{\varsigma-1}\wp^{\chi-1}-\int_0^{t_x}(t-\wp)^{\varsigma-1}\wp^{\chi-1}\right]\\ &\quad\times\left(\lambda_X\varpi+\beth_X\right)\\ &\leq \frac{\lambda_X\chi+\beth_A}{\mathscr{A}\mathscr{B}(\varsigma)\Gamma(\varsigma)}\left[t_2^{\varsigma,\chi}-t_1^{\varsigma,\chi}\right] \end{aligned} \tag{24}$$

Similarly,

$$\begin{aligned} \left|Y_2(t_2,I)-Y_2(t_1,I)\right| &\leq \frac{\lambda_B\varpi+\beth_B}{\mathscr{A}\mathscr{B}(\varsigma)\Gamma(\varsigma)}\left(t_2^{\varsigma,\chi}-t_1^{\varsigma,\chi}\right),\\ \left|Z_2(t_2,\beta)-Z_2(t_1,\beta)\right| &\leq \frac{\lambda_Z\varpi+\beth_Z}{\mathscr{A}\mathscr{B}(\varsigma)\Gamma(\varsigma)}\left(t_2^{\varsigma,\chi}-t_1^{\varsigma,\chi}\right). \end{aligned} \tag{25}$$

As $t_2\to t_1$ is independent of (G,I,β). This implies that

$$\left\|h(X_2,Y_2,Z_2)(t_2)-h(X_2,Y_2,Z_2)(t_1)\right\|\to 0 \tag{26}$$

$\Rightarrow$ $h(X_2,Y_2,Z_2)$ indicates an equi-continuous, completely continuous operator.

$\Rightarrow$ $h(X_2,Y_2,Z_2)$ it is reasonably concise, according to Arzela's theorem.

The Krasnoselski theorem implies that the compactness of the operators Q and V ensures the existence of a unique singular solution. □

Theorem 4.2. *The solution of the model (9) is considered unique if*

$$\frac{F^{\varsigma,\chi}}{\mathscr{A}\mathscr{B}(\varsigma)\Gamma(\varsigma)}\mathscr{W}\leq 1, \tag{27}$$

where $\mathscr{W} = \max\{\mathscr{M}_X, \mathscr{W}_Y, \mathscr{M}_Z.\}$

Proof. Establish an operator $\mathscr{Q} = (\mathscr{Q}_1,\mathscr{Q}_2,\mathscr{Q}_3) : \mathbb{Z}\to\mathbb{Z}$ utilizing (22) as:

$$\begin{aligned} \mathscr{Q}_1(G)(t) &= G(0)+\frac{\chi(1-\varsigma)t^{\chi-1}}{\mathscr{A}\mathscr{B}(\varsigma)}X(t,G(t))\\ &\quad+\frac{\varsigma\chi}{\mathscr{A}\mathscr{B}(\varsigma)\Gamma(\varsigma)}\int_0^t(t-\wp)^{\varsigma-1}\wp^{\chi-1}X(\wp,G(\wp))d\wp,\\ \mathscr{Q}_2(I)(t) &= I(0)+\frac{\chi(1-\varsigma)t^{\chi-1}}{\mathscr{A}\mathscr{B}(\varsigma)}Y(t,I(t))\\ &\quad+\frac{\varsigma\chi}{\mathscr{A}\mathscr{B}(\varsigma)\Gamma(\varsigma)}\int_0^t(t-\wp)^{\varsigma-1}\wp^{\chi-1}Y(\wp,I(\wp))d\wp,\\ \mathscr{Q}_3(\beta)(t) &= \beta(0)+\frac{\chi(1-\varsigma)t^{\chi-1}}{\mathscr{A}\mathscr{B}(\varsigma)}Z(t,\beta(t))\\ &\quad+\frac{\varsigma\chi}{\mathscr{A}\mathscr{B}(\varsigma)\Gamma(\varsigma)}\int_0^t(t-\wp)^{\varsigma-1}\wp^{\chi-1}Z(\wp,\beta(\wp))d\wp. \end{aligned} \tag{28}$$

For (G,I,β), $(\bar{G},\bar{I},\bar{\beta})\in\mathbb{Z}$, and utilizing (28) we have,

$$\begin{aligned} \left\|\mathscr{Q}_1(G)(t)-\mathscr{Q}_1(\bar{G})(t)\right\| &= \frac{\chi(1-\varsigma)t^{\chi-1}}{\mathscr{A}\mathscr{B}(\varsigma)}\|\mathscr{A}(t,G(t))-X(t,\bar{G}(t))\|\\ &\quad+\frac{\varsigma\chi}{\mathscr{A}\mathscr{B}(\varsigma)\Gamma(\varsigma)}\int_0^t\|X(\wp,G(\wp))-X(\wp,\bar{G}(\wp))\|\\ &\quad\times(t-\wp)^{\varsigma-1}\wp^{\chi-1}X(\wp,G(\wp))d\wp\\ &\leq \frac{\chi(1-\varsigma)t^{\chi-1}}{\mathscr{A}\mathscr{B}(\varsigma)}\mathscr{W}_X\\ &\quad\times\|G-\bar{G}\|+\frac{\wp^{\varsigma,\chi}}{\mathscr{A}\mathscr{B}(\varsigma)\Gamma(\varsigma)}\mathscr{W}_X\|G-\bar{G}\|\\ &\leq\left[\frac{\chi(1-\varsigma)t^{\chi-1}}{\mathscr{A}\mathscr{B}(\varsigma)}+\frac{\wp^{\varsigma,\chi}}{\mathscr{A}\mathscr{B}(\varsigma)\Gamma(\varsigma)}\right]\mathscr{W}_X\|G-\bar{G}\| \end{aligned} \tag{29}$$

$\|G-\bar{G}\|\to 0$ when $G\to\bar{G}$. Hence

$$\left\|\mathscr{Q}_1(G)(t)-\mathscr{Q}_1(\bar{G})(t)\right\|\leq\left[\frac{\chi(1-\varsigma)t^{\chi-1}}{\mathscr{A}\mathscr{B}(\varsigma)}+\frac{\wp^{\varsigma,\chi}}{\mathscr{A}\mathscr{B}(\varsigma)\Gamma(\varsigma)}\right]\mathscr{W}_X\leq 1 \tag{30}$$

with

$$\left\|\mathscr{Q}_1(G)(t)-\mathscr{Q}_1(\bar{G})(t)\right\|\left[1-\left(\frac{\chi(1-\varsigma)t^{\chi-1}}{\mathscr{A}\mathscr{B}(\varsigma)}+\frac{\wp^{\varsigma,\chi}}{\mathscr{A}\mathscr{B}(\varsigma)\Gamma(\varsigma)}\right)\mathscr{W}_X\right]\leq 0. \tag{31}$$

Using this approach, we find

$$\begin{aligned} &\left\|\mathscr{Q}(G,I,\beta)(t)-\mathscr{Q}(\bar{G},\bar{I},\bar{\beta})(t)\right\|\\ &\leq\left(\frac{\chi(1-\varsigma)t^{\chi-1}}{\mathscr{A}\mathscr{B}(\varsigma)}+\frac{\wp^{\varsigma,\chi}}{\mathscr{A}\mathscr{B}(\varsigma)\Gamma(\varsigma)}\right)\mathscr{W}\left\|(G,I,\beta)-(\bar{G},\bar{I},\bar{\beta})\right\| \end{aligned} \tag{32}$$

Mapping contractions it is confirmed that our suggested model has a unique fixed-point solution by $\mathbb{Q}$, which combines the features of both the Schauder and Krasnoselski theorems.

Remark 1. The fixed-point method applied in the paper plays an important role in the proof of the existence and uniqueness of the fractional-order model. Therefore, it reformulates the differential equations of the model into a fixed-point problem and then manages to guarantee that the system has a unique solution according to Krasnoselski's fixed-point theorem. This has given the model a strong mathematical background that when applied in simulating and analyzing the insulin and glucose in the body under different conditions can be done confidently. □

5. Ulam–Hyers stability

The stability analysis of the suggested fractional-order diabetes mellitus model in term of the Ulam–Hyers technique means that small disturbances does not cause vast oscillation within the proposed model making the model more accurate. This stability is important especially

in the case of PID controller in regulating of blood glucose levels under different physiological conditions. Therefore, it is important to incorporate Ulam–Hyers stability in our model not only for the theoretical implications, but more importantly for the realistic applications.

$$\begin{aligned}
&\left| G(t) + \left(\frac{\chi(1-\varsigma)t^{\chi-1}}{\mathscr{A}\mathscr{B}(\varsigma)} \right) \eta_1(t, G(t)) \right. \\
&\quad \left. + \left(\frac{\varsigma\chi}{\mathscr{A}\mathscr{B}(\varsigma)} \int_0^t (t-\wp)\wp^{\varsigma-1} \eta_1(t, G(t))\, d\wp \right) \right| \leq \varpi_1 \\
&\left| I(t) + \left(\frac{\chi(1-\varsigma)t^{\chi-1}}{\mathscr{A}\mathscr{B}(\varsigma)} \right) \eta_2(t, I(t)) \right. \\
&\quad \left. + \left(\frac{\varsigma\chi}{\mathscr{A}\mathscr{B}(\varsigma)} \int_0^t (t-\wp)\wp^{\varsigma-1} \eta_2(t, I(t))\, d\wp \right) \right| \leq \varpi_2 \\
&\left| \beta(t) + \left(\frac{\chi(1-\varsigma)t^{\chi-1}}{\mathscr{A}\mathscr{B}(\varsigma)} \right) \eta_3(t, \beta(t)) \right. \\
&\quad \left. + \left(\frac{\varsigma\chi}{\mathscr{A}\mathscr{B}(\varsigma)} \int_0^t (t-\wp)\wp^{\varsigma-1} \eta_3(t, \beta(t))\, d\wp \right) \right| \leq \varpi_3.
\end{aligned} \tag{33}$$

there exist $\bar{G}, \bar{I}$ *and* $\bar{\beta}$ satisfying

$$\begin{aligned}
\bar{G}(t) &= \left(\frac{\chi(1-\varsigma)t^{\chi-1}}{\mathscr{A}\mathscr{B}(\varsigma)} \right) \eta_1\left(t, \bar{G}(t)\right) \\
&\quad + \left(\frac{\varsigma\chi}{\mathscr{A}\mathscr{B}(\varsigma)} \int_0^t (t-\wp)\wp^{\varsigma-1} \eta_1\left(t, \bar{G}(t)\right) d\wp, \right. \\
\bar{I}(t) &= \left(\frac{\chi(1-\varsigma)t^{\chi-1}}{\mathscr{A}\mathscr{B}(\varsigma)} \right) \eta_2\left(t, \bar{I}(t)\right) \\
&\quad + \left(\frac{\varsigma\chi}{\mathscr{A}\mathscr{B}(\varsigma)} \int_0^t (t-\wp)\wp^{\varsigma-1} \eta_1\left(t, \bar{I}(t)\right) d\wp, \right. \\
\bar{\beta}(t) &= \left(\frac{\chi(1-\varsigma)t^{\chi-1}}{\mathscr{A}\mathscr{B}(\varsigma)} \right) \eta_3\left(t, \bar{\beta}(t)\right) \\
&\quad + \left(\frac{\varsigma\chi}{\mathscr{A}\mathscr{B}(\varsigma)} \int_0^t (t-\wp)\wp^{\varsigma-1} \eta_1\left(t, \bar{\beta}(t)\right) d\wp, \right.
\end{aligned} \tag{34}$$

such that

$$\begin{aligned}
&G(t) - \bar{G} \leq \varpi_1 \Omega_1, \\
&I(t) - \bar{I} \leq \varpi_2 \Omega_2, \\
&\beta(t) - \bar{\beta} \leq \varpi_3 \Omega_3.
\end{aligned} \tag{35}$$

Theorem 5.1. *Consider that* $G(t), I(t), \beta(t)$ *and* $\bar{G}(t), \bar{I}(t), \bar{\beta}(t)$ *are functions that remain consistent such that*

$$\|G(t)\| \leq \lambda_1, \|I(t)\| \leq \lambda_2, \|\beta(t)\| \leq \lambda_3 \tag{36}$$

Ulam–Hyers stability for the fractional model (9) exists if this condition is met.

Proof. A solution has been identified for $G(t), I(t)$ *and* $\beta(t)$. Assume that $\bar{G}(t), \bar{I}(t), \bar{\beta}(t)$ are the approximate solutions to our system and they meet the requirements mentioned below.

$$\begin{aligned}
\left\| G(t) - \bar{G}(t) \right\| &\leq \frac{\chi(1-\varsigma)t^{\chi-1}}{\mathscr{A}\mathscr{B}(\varsigma)} \lambda_1\left(t, \bar{G}(t)\right) \\
&\quad + \frac{\varsigma\chi}{\mathscr{A}\mathscr{B}(\varsigma)} \int_0^t (t-\wp)^{\varsigma-1} \lambda_1\left(t, \bar{G}(t)\right) d\wp \\
&\leq \frac{\chi(1-\varsigma)t^{\chi-1} + \varsigma\chi}{\mathscr{A}\mathscr{B}(\varsigma)} \lambda_1 \left\| G(t) - \bar{G}(t) \right\|
\end{aligned} \tag{37}$$

consider $\lambda_i = \varpi_i$ and $\Omega_i = \frac{\chi(1-\varsigma)t^{\chi-1}+\varsigma\chi}{\mathscr{A}\mathscr{B}(\varsigma)}$ for $i = 1, 2, 3$ we have

$$\left\| G(t) - \bar{G}(t) \right\| \leq \varpi_1 \Omega_1 \tag{38}$$

similarly,

$$\begin{aligned}
\left\| I(t) - \bar{I}(t) \right\| &\leq \frac{\chi(1-\varsigma)t^{\chi-1}}{\mathscr{A}\mathscr{B}(\varsigma)} \lambda_2\left(t, \bar{I}(t)\right) \\
&\quad + \frac{\varsigma\chi}{\mathscr{A}\mathscr{B}(\varsigma)} \int_0^t (t-\wp)^{\varsigma-1} \lambda_2\left(t, \bar{I}(t)\right) d\wp \\
&\leq \frac{\chi(1-\varsigma)t^{\chi-1} + \varsigma\chi}{\mathscr{A}\mathscr{B}(\varsigma)} \lambda_2 \left\| I(t) - \bar{I}(t) \right\| \leq \varpi_2 \Omega_2
\end{aligned} \tag{39}$$

and

$$\begin{aligned}
\left\| \beta(t) - \bar{\beta}(t) \right\| &\leq \frac{\chi(1-\varsigma)t^{\chi-1}}{\mathscr{A}\mathscr{B}(\varsigma)} \lambda_3\left(t, \bar{\beta}(t)\right) \\
&\quad + \frac{\varsigma\chi}{\mathscr{A}\mathscr{B}(\varsigma)} \int_0^t (t-\wp)^{\varsigma-1} \lambda_3\left(t, \bar{\beta}(t)\right) d\wp \\
&\leq \frac{\chi(1-\varsigma)t^{\chi-1} + \varsigma\chi}{\mathscr{A}\mathscr{B}(\varsigma)} \lambda_2 \left\| \beta(t) - \bar{\beta}(t) \right\| \leq \varpi_3 \Omega_3
\end{aligned} \tag{40}$$

The Ulam–Hyers stability of the system is demonstrated by these differences.

6. PID and controllability

The diabetes mellitus model was examined in [31]. The diabetes mellitus mathematical model is provided as

$$\begin{cases}
\dot{G}(t) = R_0 + G_e - \left(E_{GO} - S_I I(t-\tau) \right) G(t-\tau), \\
\dot{I}(t) = \frac{\beta\sigma G^2(t-\tau)}{(\alpha+G^2(t-\tau))} - (\rho - K) I(t-\tau), \\
\dot{\beta}(t) = \left(-d_0 + r_1 G(t-\tau) + r_2 G^2(t-\tau) \right) \beta(t-\tau),
\end{cases} \tag{41}$$

In this work, we develop a fractal–fractional model for diabetes mellitus utilizing the Mittag-Leffler kernel. This model is characterized as follows:

$$\begin{cases}
{}^{FFM}D_{0,t}^{\varsigma,\chi} G(t) = R_0 + G_e - \left(E_{GO} - S_I I(t-\tau) \right) G(t-\tau), \\
{}^{FFM}D_{0,t}^{\varsigma,\chi} I(t) = \frac{\beta\sigma G^2(t-\tau)}{(\alpha+G^2(t-\tau))} - (\rho - K) I(t-\tau), \\
{}^{FFM}D_{0,t}^{\varsigma,\chi} \beta(t) = \left(-d_0 + r_1 G(t-\tau) + r_2 G^2(t-\tau) \right) \beta(t-\tau),
\end{cases} \tag{42}$$

where $0 < \chi \leq 1$.

The fractional-order PID controller outperforms traditional PID controllers in terms of performance, stability, and adaptability, particularly in managing the complex and dynamic nature of insulin–glucose regulation. Its ability to incorporate memory effects, handle nonlinearities, and adapt to varying patient conditions makes it a superior choice for personalized diabetes management. While other advanced control strategies like MPC and FLC offer their own benefits, the fractional-order PID controller provides a balanced approach that combines effectiveness with ease of implementation, making it a valuable tool for both researchers and clinicians in the field of diabetes care.

Remark 2. In the context of the Riemann–Liouville derivative, the Laplace transform is contingent upon its initial value. However, the Laplace transform of the ABC derivative is solely linked to the initial value of the integer derivative. It is known that the initial value of the Riemann–Liouville derivative is hard to calculate, but it is easy to determine the first value of the integer derivative. As a result, FFM is applied often in engineering. The model (42) is described using FFM.

Remark 3. The fractional-order derivative serves as a connection between two points, while the integer-order derivative can be likened to individual, distinct points in a system. Studies have demonstrated that the fractional-order derivative is more accurate in simulating real networks and possesses memory and hereditariness properties. Furthermore, fractional-order derivatives can encompass the characteristics of integer-order derivatives and are more universal. As a result, model (42) is chosen since it can faithfully capture the characteristics of memory and heredity in model. But the conventional integer-order model (41) is unable to achieve this. Furthermore, the suggested model (41) simplifies to the integral-order model (42) when $\varsigma = 1$. The

similar positive equilibrium and structure are shared by the classic model (41) and the fractional model (42). The following is the design of the fractional-order PID controller:

$$\begin{aligned} u(t) &= k_p e(t) + k_{i0} J_t^{-\chi} e(t) + k_d {}^{FFM}D_{0,t}^{\varsigma,\chi} e(t), \\ u_1(t) &= k_p a(t) + k_{i0} J_t^{-\chi} a(t) + k_d {}^{FFM}D_{0,t}^{\varsigma,\chi} a(t), \\ u_2(t) &= k_p c(t) + k_{i0} J_t^{-\chi} c(t) + k_d {}^{FFM}D_{0,t}^{\varsigma,\chi} c(t), \end{aligned} \tag{43}$$

where $e(t) = (G(t) - G^*)$, $a(t) = (I(t) - I^*)$ and $c(t) = (\beta(t) - \beta^*)$, and k_p, k_i and k_d are the control gains.

Remark 4. In the system controller (43), the terms k_pe(t), $k_{i0} J_t^{-\varsigma} e(t)$, $k_{i0} J_t^{-\varsigma} a(t)$, $k_{i0} J_t^{-\varsigma} c(t)$, $k_d {}^{FFM}D_{0,t}^{\varsigma,\chi} e(t)$, $k_d {}^{FFM}D_{0,t}^{\varsigma,\chi} a(t)$, and $k_d {}^{FFM}D_{0,t}^{\varsigma,\chi} c(t)$ represent the proportional, integral, and derivative components, respectively. Here, k_p, k_i, and k_d are the corresponding control gains. When $k_i = 0$, the controller (43) becomes a fractional-order PD controller. Similarly, when $k_d = 0$, it reduces to a fractional PI controller. For $\varsigma = 1$, the controller (43) functions as a conventional integral-order PID controller.

Remark 5. Numerous bifurcation control strategies have been developed for both fractional-order and integral-order systems, including the hybrid control, washout filter control, time-delayed feedback control, and dynamic state feedback control. In recent studies, the fractional-order PD controller was utilized to achieve effective bifurcation control for fractional systems with delays. Research indicates that the integer-order PID control outperforms the integer-order PD control in minimizing interference and reducing the steady-state error of the controlled system. Moreover, it has been noted that the integer-order PD control may lead to different equilibrium points; however, this challenge can be effectively addressed by employing the integer-order PID control. In this study, we introduce the generic fractional-order PID feedback synthesis for the first time, aiming to achieve bifurcation management of the fractional diabetes model.

The controlled model that results from applying controller (43) to model (42) is as follows:

$$\begin{aligned} {}^{FFM}D_{0,t}^{\varsigma,\chi} G(t) &= R_0 + G_e - \left(E_{GO} - S_I I(t-\tau)\right) G(t-\tau) + u(t), \\ {}^{FFM}D_{0,t}^{\varsigma,\chi} I(t) &= \frac{\beta\sigma G^2(t-\tau)}{\left(\alpha + G^2(t-\tau)\right)} - (\rho - K) I(t-\tau) + u_1(t), \\ {}^{FFM}D_{0,t}^{\varsigma,\chi} \beta(t) &= \left(-d_0 + r_1 G(t-\tau) + r_2 G^2(t-\tau)\right) \beta(t-\tau) + u_2(t), \end{aligned} \tag{44}$$

Declare the new variables.

$$\begin{aligned} A(t) &= {}_0J_t^{-\chi} e(t), \\ V(t) &= {}_0J_t^{-\chi} a(t), \\ W(t) &= {}_0J_t^{-\chi} c(t), \end{aligned}$$

$$\begin{aligned} {}^{FFM}D_{0,t}^{\varsigma,\chi} A(t) &= e(t), \\ {}^{FFM}D_{0,t}^{\varsigma,\chi} V(t) &= a(t), \\ {}^{FFM}D_{0,t}^{\varsigma,\chi} W(t) &= c(t). \end{aligned}$$

Consequently, it is possible to formulate the fractional-order controlled model (44) as

$$\begin{aligned} {}^{FFM}D_{0,t}^{\varsigma,\chi} G(t) &= \left[R_0 + G_e - \left(E_{GO} - S_I I(t-\tau)\right) G(t-\tau) \right. \\ &\quad \left. + k_p \left(G(t) - G^*\right) + k_i A(t)\right] \frac{1}{1-k_d}, \\ {}^{FFM}D_{0,t}^{\varsigma,\chi} I(t) &= \left[\frac{\beta\sigma G^2(t-\tau)}{\left(\alpha + G^2(t-\tau)\right)} - (\rho - K) I(t-\tau) \right. \\ &\quad \left. + k_p \left(I(t) - I^*\right) + k_i V(t)\right] \frac{1}{1-k_d}, \\ {}^{FFM}D_{0,t}^{\varsigma,\chi} \beta(t) &= \left[\left(-d_0 + r_1 G(t-\tau) + r_2 G^2(t-\tau)\right) \beta(t-\tau) \right. \\ &\quad \left. + k_p \left(\beta(t) - \beta^*\right) + k_i W(t)\right] \frac{1}{1-k_d}, \end{aligned} \tag{45}$$

$$\begin{aligned} {}^{FFM}D_{0,t}^{\varsigma,\chi} A(t) &= \left(G(t) - G^*\right), \\ {}^{FFM}D_{0,t}^{\varsigma,\chi} V(t) &= \left(I(t) - I^*\right), \\ {}^{FFM}D_{0,t}^{\varsigma,\chi} W(t) &= \left(\beta(t) - \beta^*\right). \end{aligned}$$

Remark 6. The direct examination of the dynamical characteristics of the controlled model (44) presents challenges due to the presence of an integral variable ${}^{FFM}D_{0,t}^{\varsigma,\chi} e(t)$, ${}^{FFM}D_{0,t}^{\varsigma,\chi} a(t)$, ${}^{FFM}D_{0,t}^{\varsigma,\chi} c(t)$ in the controller (43). Consequently, we leverage variable transformation to simplify the controlled model (44), making it more amenable to analysis, and obtain the commensurate-order model (45).

Remark 7. The unique positive equilibrium of the controlled model (45) is represented by $(G^\bullet, 0)^T$, $(I^\bullet, 0)^T$, $(\beta^\bullet, 0)^T$. It is important to note that the first component of the vectors $(G^\bullet, 0)^T$, $(I^\bullet, 0)^T$, $(\beta^\bullet, 0)^T$ yields $G^\bullet$, $I^\bullet$, and $\beta^\bullet$, providing the unique positive equilibrium of the uncontrolled model (43). Consequently, our proposed fractional-order PID controller (44) effectively maintains the unique equilibrium of model (43).

7. Numerical scheme

In this section, we will utilize the two-step Lagrange polynomial to numerically solve the system (9). The fractional-order PID controller model for insulin–glucose dynamics was solved using a two-step Lagrange polynomial method. This method is well-suited for fractional-order differential equations as it provides a robust approximation of the solution by fitting polynomials to the data points.

$$\begin{cases} {}^{FFM}D_{0,t}^{\varsigma,\chi} G(t) = R_0 + G_e - \left(E_{GO} - S_I I\right) G, \\ {}^{FFM}D_{0,t}^{\varsigma,\chi} I(t) = \frac{\beta\sigma G^2}{(\alpha+G^2)} - (\rho - K) I, \\ {}^{FFM}D_{0,t}^{\varsigma,\chi} \beta(t) = \left(-d_0 + r_1 G + r_2 G^2\right) \beta, \end{cases} \tag{46}$$

To keep things simple, we can depict the previously given system as follows:

$$\begin{aligned} {}^{FFM}\mathrm{D}_{0,t}^{\varsigma,\chi} G(t) &= \mathrm{ך}_1[t, G, I, \beta], \\ {}^{FFM}\mathrm{D}_{0,t}^{\varsigma,\chi} I(t) &= \mathrm{ך}_2[t, G, I, \beta], \\ {}^{FFM}\mathrm{D}_{0,t}^{\varsigma,\chi} \beta(t) &= \mathrm{ך}_3[t, G, I, \beta]. \end{aligned} \tag{47}$$

After applying the fractal–fractional integral with the Mittag-Leffler kernel, we obtain the following:

$$\begin{aligned} G(t_k+1) &= G(0) + \frac{1-\varsigma}{\mathscr{AB}(\varsigma)} t_k^{1-\chi} \mathrm{ך}_1\left[(t_k, G(t_k), I(t_k), \beta(t_k))\right] \\ &\quad + \frac{\varsigma}{\mathscr{AB}(\varsigma)\Gamma(\varsigma)} \sum_{i=2}^{k} \int_{t_i}^{t_{i+1}} \mathrm{ך}_1(t, G, I, \beta) \wp^{1-\chi} (t_{k+1} - \wp)^{\varsigma-1} d\wp \end{aligned} \tag{48}$$

$$\begin{aligned} I(t_k+1) &= I(0) + \frac{1-\varsigma}{\mathscr{AB}(\varsigma)} t_k^{1-\chi} \mathrm{ך}_2\left[(t_k, G(t_k), I(t_k), \beta(t_k))\right] \\ &\quad + \frac{\varsigma}{\mathscr{AB}(\varsigma)\Gamma(\varsigma)} \sum_{i=2}^{k} \int_{t_i}^{t_{i+1}} \mathrm{ך}_2(t, G, I, \beta) \wp^{1-\chi} (t_{k+1} - \wp)^{\varsigma-1} d\wp \end{aligned} \tag{49}$$

$$\begin{aligned} \beta(t_k+1) &= \beta(0) + \frac{1-\varsigma}{\mathscr{AB}(\varsigma)} t_k^{1-\chi} \mathrm{ך}_3\left[(t_k, G(t_k), I(t_k), \beta(t_k))\right] \\ &\quad + \frac{\varsigma}{\mathscr{AB}(\varsigma)\Gamma(\varsigma)} \sum_{i=2}^{k} \int_{t_i}^{t_{i+1}} \mathrm{ך}_3(t, G, I, \beta) \wp^{1-\chi} (t_{k+1} - \wp)^{\varsigma-1} d\wp \end{aligned} \tag{50}$$

In this case, we review the Newton polynomial:

$$\begin{aligned} \mathfrak{F}(t, G, I, \beta) \simeq\ & \mathfrak{F}(t_{k-2}, G_{k-2}, I_{k-2}, \beta_{k-2}) + \frac{1}{\Delta t}\left[\mathfrak{F}(t_{k-1}, G_{k-1}, I_{k-1}, \beta_{k-1}) \right. \\ & \left. - \mathfrak{F}(t_{k-2}, G_{k-2}, I_{k-2}, \beta_{k-2})\right] \\ & \times (\wp - t_{k-2}) + \frac{1}{2\Delta t^2}\left[\mathfrak{F}(t_k, G_k, I_k, \beta_k)\right. \end{aligned}$$

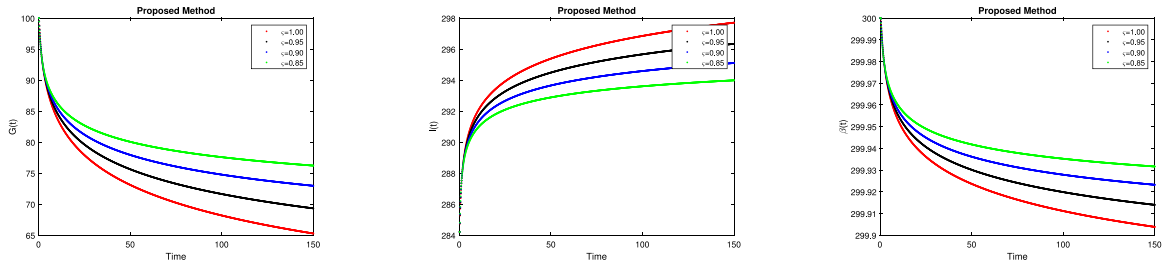

(a) (b) (c)

Fig. 1. Simulation of $G(t), I(t), \beta(t)$ at G = 300.

$$- 2\mathfrak{F}(t_{k-1}, G_{k-1}, I_{k-1}, \beta_{k-1}) - \mathfrak{F}(t_{k-2}, G_{k-2}, I_{k-2}, \beta_{k-2})\Big] \times (\wp - t_{k-2})(\wp - t_{k-1})$$

Eqs. (48)–(50) can be solved using the Newton polynomial. This gives us

$$\begin{aligned}
G_{(k+1)} &= G(0) + \frac{1-\varsigma}{\mathscr{A}\mathscr{B}(\varsigma)} t_k^{1-\chi} \daleth_1\left(t_k, G(t_k), I(t_k), \beta(t_k)\right) \\
&+ \frac{\varsigma}{\mathscr{A}\mathscr{B}(\varsigma)\Gamma(\varsigma)} \sum_{i=2}^{k} \daleth_1\left(t_{i-2}, G^{i-2}, I^{i-2}, \beta^{i-2}\right) t_{i-2}^{1-\chi} \\
&\times \int_{t_i}^{t_{i+1}} (t_{k+1} - \varphi)^{\varsigma-1} d\varphi \\
&+ \frac{\varsigma}{\mathscr{A}\mathscr{B}(\varsigma)\Gamma(\varsigma)} \sum_{i=2}^{k} \frac{1}{\Delta t} \Big[t_{i-1}^{1-\chi} \ \daleth_1\left(t_{i-1}, G^{i-1}, I^{i-1}, \beta^{i-1}\right) \\
&- t_{i-2}^{1-\chi} \ \daleth_1\left(t_{i-2}, G^{i-2}, I^{i-2}, \beta^{i-2}\right) \Big] \\
&\times \int_{t_i}^{t_{i+1}} (\wp - t_{i-2})(t_{k+1} - \wp)^{\varsigma-1} d\wp \\
&+ \frac{\varsigma}{\mathscr{A}\mathscr{B}(\varsigma)\Gamma(\varsigma)} \sum_{i=2}^{k} \frac{1}{2\Delta t^2} \Big[t_i^{1-\chi} \daleth_1\left(t_i, G^i, I^i, \beta^i\right) \\
&- 2t_{i-1}^{1-\chi} \daleth_1\left(t_{i-1}, G^{i-1}, I^{i-1}, \beta^{i-1}\right) \\
&+ t_{i-2}^{1-\chi} \daleth_1\left(t_{i-2}, G^{i-2}, I^{i-2}, \beta^{i-2}\right) \Big] \\
&\times \int_{t_i}^{t_{i+1}} (\wp - t_{i-2})(\wp - t_{i-1})(t_{k+1} - \wp)^{\varsigma-1} d\wp
\end{aligned} \tag{51}$$

$$\begin{aligned}
I_{(k+1)} &= I(0) + \frac{1-\varsigma}{\mathscr{A}\mathscr{B}(\varsigma)} t_k^{1-\chi} \daleth_2\left(t_k, G(t_k), I(t_k), \beta(t_k)\right) \\
&+ \frac{\varsigma}{\mathscr{A}\mathscr{B}(\varsigma)\Gamma(\varsigma)} \sum_{i=2}^{k} \daleth_2\left(t_{i-2}, G^{i-2}, I^{i-2}, \beta^{i-2}\right) t_{i-2}^{1-\chi} \\
&\times \int_{t_i}^{t_{i+1}} (t_{k+1} - \varphi)^{\varsigma-1} d\varphi \\
&+ \frac{\varsigma}{\mathscr{A}\mathscr{B}(\varsigma)\Gamma(\varsigma)} \sum_{i=2}^{k} \frac{1}{\Delta t} \Big[t_{i-1}^{1-\chi} \ \daleth_2\left(t_{i-1}, G^{i-1}, I^{i-1}, \beta^{i-1}\right) \\
&- t_{i-2}^{1-\chi} \ \daleth_2\left(t_{i-2}, G^{i-2}, I^{i-2}, \beta^{i-2}\right) \Big] \\
&\times \int_{t_i}^{t_{i+1}} (\wp - t_{i-2})(t_{k+1} - \wp)^{\varsigma-1} d\wp \\
&+ \frac{\varsigma}{\mathscr{A}\mathscr{B}(\varsigma)\Gamma(\varsigma)} \sum_{i=2}^{k} \frac{1}{2\Delta t^2} \Big[t_i^{1-\chi} \daleth_2\left(t_i, G^i, I^i, \beta^i\right) \\
&- 2t_{i-1}^{1-\chi} \daleth_2\left(t_{i-1}, G^{i-1}, I^{i-1}, \beta^{i-1}\right) \\
&+ t_{i-2}^{1-\chi} \daleth_2\left(t_{i-2}, G^{i-2}, I^{i-2}, \beta^{i-2}\right) \Big] \\
&\times \int_{t_i}^{t_{i+1}} (\wp - t_{i-2})(\wp - t_{i-1})(t_{k+1} - \wp)^{\varsigma-1} d\wp
\end{aligned} \tag{52}$$

$$\begin{aligned}
\beta_{(k+1)} &= \beta(0) + \frac{1-\varsigma}{\mathscr{A}\mathscr{B}(\varsigma)} t_k^{1-\chi} \daleth_3\left(t_k, G(t_k), I(t_k), \beta(t_k)\right) \\
&+ \frac{\varsigma}{\mathscr{A}\mathscr{B}(\varsigma)\Gamma(\varsigma)} \sum_{i=2}^{k} \daleth_3\left(t_{i-2}, G^{i-2}, I^{i-2}, \beta^{i-2}\right) t_{i-2}^{1-\chi} \\
&\times \int_{t_i}^{t_{i+1}} (t_{k+1} - \varphi)^{\varsigma-1} d\varphi \\
&+ \frac{\varsigma}{\mathscr{A}\mathscr{B}(\varsigma)\Gamma(\varsigma)} \sum_{i=2}^{k} \frac{1}{\Delta t} \Big[t_{i-1}^{1-\chi} \ \daleth_3\left(t_{i-1}, G^{i-1}, I^{i-1}, \beta^{i-1}\right) \\
&- t_{i-2}^{1-\chi} \ \daleth_3\left(t_{i-2}, G^{i-2}, I^{i-2}, \beta^{i-2}\right) \Big] \\
&\times \int_{t_i}^{t_{i+1}} (\wp - t_{i-2})(t_{k+1} - \wp)^{\varsigma-1} d\wp \\
&+ \frac{\varsigma}{\mathscr{A}\mathscr{B}(\varsigma)\Gamma(\varsigma)} \sum_{i=2}^{k} \frac{1}{2\Delta t^2} \Big[t_i^{1-\chi} \daleth_3\left(t_i, G^i, I^i, \beta^i\right) \\
&- 2t_{i-1}^{1-\chi} \daleth_3\left(t_{i-1}, G^{i-1}, I^{i-1}, \beta^{i-1}\right) \\
&+ t_{i-2}^{1-\chi} \daleth_3\left(t_{i-2}, G^{i-2}, I^{i-2}, \beta^{i-2}\right) \Big] \\
&\times \int_{t_i}^{t_{i+1}} (\wp - t_{i-2})(\wp - t_{i-1})(t_{k+1} - \wp)^{\varsigma-1} d\wp
\end{aligned} \tag{53}$$

The following computations can be used to find the integrals in the Eqs. (51)–(53).

$$\begin{aligned}
&\int_{t_i}^{t_{i+1}} (t_{k+1} - \wp)^{\varsigma-1} d\wp = \frac{(\Delta t)^{\varsigma}}{\varsigma} \left[(k-i+1)^{\varsigma} - (k-i)^{\varsigma}\right] \\
&\int_{t_i}^{t_{i+1}} (\wp - t_{i-2})(t_{k+1} - \wp)^{\varsigma-1} d\wp = \frac{(\Delta t)^{\varsigma+1}}{\varsigma(\varsigma+1)} \Big[(k-i+1)^{\varsigma}(k-i+3+2\varsigma) \\
&\quad - (k-i)^{\varsigma}(k-i+3+3\varsigma)\Big] \\
&\int_{t_i}^{t_{i+1}} (\wp - t_{i-2})(\wp - t_{i-1})(t_{k+1} - \wp)^{\varsigma-1} d\wp = \frac{(\Delta t)^{\varsigma+2}}{\varsigma(\varsigma+1)(\varsigma+2)} \\
&\quad \times \Big[(k-i+1)^{\varsigma}\Big\{2(k-i)^2 + (3\varsigma+10) \\
&(k-i) + 2\varsigma^2 + 9\varsigma + 12\Big\} - (k-i)^{\varsigma}\Big\{2(k-i)^2 + (5\varsigma+10)(k-i) \\
&\quad + 6\varsigma^2 + 18\varsigma + 12\Big\}\Big]
\end{aligned} \tag{54}$$

As a result, we finally get

$$\begin{aligned}
G(k+1) &= G(0) + \frac{1-\varsigma}{\mathscr{A}\mathscr{B}(\varsigma)} t_k^{1-\chi} \daleth_1\left[t_k, G(t_k), I(t_k), \beta(t_k)\right] \\
&+ \frac{\varsigma(\Delta t)^{\varsigma}}{\mathscr{A}\mathscr{B}(\varsigma)\Gamma(\varsigma+1)} \sum_{i=2}^{k} \daleth_1\left[t_{i-2}, G^{i-2}, I^{i-2}, \beta^{i-2}\right] t_{i-2}^{1-\chi} \times Y \\
&+ \frac{\varsigma(\Delta t)^{\varsigma}}{\mathscr{A}\mathscr{B}(\varsigma)\Gamma(\varsigma+2)} \sum_{i=2}^{k} \Big\{ t_{i-1}^{1-\chi} \ \daleth_1\left[t_{i-1}, G^{i-1}, I^{i-1}, \beta^{i-1}\right] \\
&- t_{i-2}^{1-\chi} \ \daleth_1\left[t_{i-2}, G^{i-2}, I^{i-2}, \beta^{i-2}\right] \Big\} \times \Phi
\end{aligned}$$

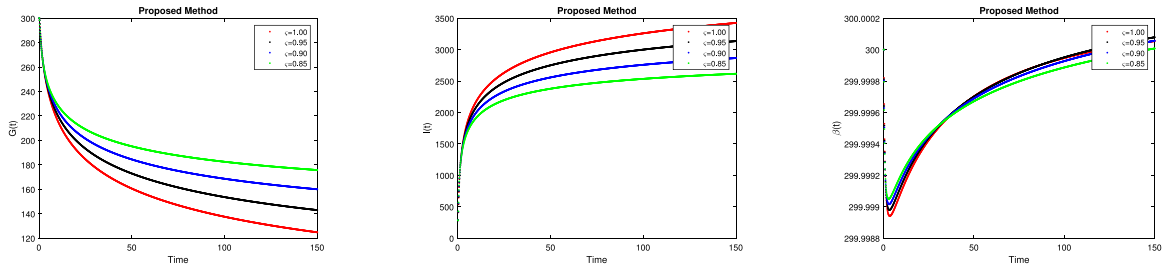

(a) (b) (c)

Fig. 2. Simulation of $G(t), I(t), \beta(t)$ at G = 600.

$$
\begin{aligned}
&+\frac{\varsigma(\Delta t)^{\varsigma}}{2\mathscr{A}\mathscr{B}(\varsigma)\Gamma(\varsigma+3)}\sum_{i=2}^{k}\Big\{\, t_i^{1-\chi}\daleth_1\left[t_i,G^i,I^i,\beta^i\right]\\
&-2t_{i-1}^{1-\chi}\daleth_1\left[t_{i-1},G^{i-1},I^{i-1},\beta^{i-1}\right]\\
&+t_{i-2}^{1-\chi}\daleth_1\left[t_{i-2},G^{i-2},I^{i-2},\beta^{i-2}\right]\Big\}\times\Psi.
\end{aligned}
\tag{55}
$$

$$
\begin{aligned}
I(k+1) &= I(0)+\frac{1-\varsigma}{\mathscr{A}\mathscr{B}(\varsigma)}t_k^{1-\chi}\daleth_2\left[t_k,G(t_k),I(t_k),\beta(t_k)\right]\\
&+\frac{\varsigma(\Delta t)^{\varsigma}}{\mathscr{A}\mathscr{B}(\varsigma)\Gamma(\varsigma+1)}\sum_{i=2}^{k}\daleth_2\left[t_{i-2},G^{i-2},I^{i-2},\beta^{i-2}\right]t_{i-2}^{1-\chi}\times Y\\
&+\frac{\varsigma(\Delta t)^{\varsigma}}{\mathscr{A}\mathscr{B}(\varsigma)\Gamma(\varsigma+2)}\sum_{i=2}^{k}\Big\{\, t_{i-1}^{1-\chi}\ \daleth_2\left[t_{i-1},G^{i-1},I^{i-1},\beta^{i-1}\right]\\
&-t_{i-2}^{1-\chi}\ \daleth_2\left[t_{i-2},G^{i-2},I^{i-2},\beta^{i-2}\right]\Big\}\times\Phi\\
&+\frac{\varsigma(\Delta t)^{\varsigma}}{2\mathscr{A}\mathscr{B}(\varsigma)\Gamma(\varsigma+3)}\sum_{i=2}^{k}\Big\{\, t_i^{1-\chi}\daleth_2\left[t_i,G^i,I^i,\beta^i\right]\\
&-2t_{i-1}^{1-\chi}\daleth_2\left[t_{i-1},G^{i-1},I^{i-1},\beta^{i-1}\right]\\
&+t_{i-2}^{1-\chi}\daleth_2\left[t_{i-2},G^{i-2},I^{i-2},\beta^{i-2}\right]\Big\}\times\Psi.
\end{aligned}
\tag{56}
$$

$$
\begin{aligned}
\beta(k+1) &= \beta(0)+\frac{1-\varsigma}{\mathscr{A}\mathscr{B}(\varsigma)}t_k^{1-\chi}\daleth_3\left[t_k,G(t_k),I(t_k),\beta(t_k)\right]\\
&+\frac{\varsigma(\Delta t)^{\varsigma}}{\mathscr{A}\mathscr{B}(\varsigma)\Gamma(\varsigma+1)}\sum_{i=2}^{k}\daleth_3\left[t_{i-2},G^{i-2},I^{i-2},\beta^{i-2}\right]t_{i-2}^{1-\chi}\times Y\\
&+\frac{\varsigma(\Delta t)^{\varsigma}}{\mathscr{A}\mathscr{B}(\varsigma)\Gamma(\varsigma+2)}\sum_{i=2}^{k}\Big\{\, t_{i-1}^{1-\chi}\ \daleth_3\left[t_{i-1},G^{i-1},I^{i-1},\beta^{i-1}\right]\\
&-t_{i-2}^{1-\chi}\ \daleth_2\left[t_{i-2},G^{i-2},I^{i-2},\beta^{i-2}\right]\Big\}\times\Phi\\
&+\frac{\varsigma(\Delta t)^{\varsigma}}{2\mathscr{A}\mathscr{B}(\varsigma)\Gamma(\varsigma+3)}\sum_{i=2}^{k}\Big\{\, t_i^{1-\chi}\daleth_3\left[t_i,G^i,I^i,\beta^i\right]\\
&-2t_{i-1}^{1-\chi}\daleth_3\left[t_{i-1},G^{i-1},I^{i-1},\beta^{i-1}\right]\\
&+t_{i-2}^{1-\chi}\daleth_3\left[t_{i-2},G^{i-2},I^{i-2},\beta^{i-2}\right]\Big\}\times\Psi.
\end{aligned}
\tag{57}
$$

where

$$
\begin{aligned}
Y &= (k-i+1)^{\varsigma}-(k-i)^{\varsigma}\\
\Phi &= (k-i+1)^{\varsigma}(k-i+3+2\varsigma)-(k-i)^{\varsigma}(k-i+3+3\varsigma)\\
\Psi &= (k-i+1)^{\varsigma}\left[2(k-i)^2+(3\varsigma+10)(k-i)+2\varsigma^2+9\varsigma+12\right]\\
&\quad-(k-i)^{\varsigma}\left[2(k-i)^2+(5\varsigma+10)(k-i)+6\varsigma^2+18\varsigma+12\right].
\end{aligned}
\tag{58}
$$

8. Results of proposed scheme

In this context, our emphasis is on the numerical solution of the fractional diabetes mellitus model. We use simulations to approximate the system solutions in order to improve the clarity of our findings. In our simulation, we take certain values for the parameters, and the overall simulation time is $t = 150$ days. The system's parameters are listed in table (1). All simulations were implemented in MATLAB, which provided the necessary computational tools for handling the complex calculations involved in fractional-order calculus. The results were visualized using MATLAB's plotting functions, allowing for a clear interpretation of the insulin–glucose dynamics under different conditions. The glucose levels are displayed over time in the graph (1a). Different lines correspond to different fractional orders. The decay rates of the glucose levels exhibit small changes as the fractional order declines. (1b) shows the evolution of the insulin response. The dynamics of insulin are affected by the fractional order; smaller fractional orders exhibit slower variations. With minimal change in various fractional orders, the beta-cell count in (1c) is very steady at 300. Glucose levels are shown in (2a) starting at 600. The fractional order affects the rate of drop in glucose levels; lower orders exhibit a slower rate of decline. A greater alteration in insulin levels is shown in (2b) than in the preceding case. A later insulin peak is the result of lower fractional orders. As in the earlier figure, beta-cell counts are still close to 300, but a little rise is apparent at lower fractional orders (2c). Shows a similar tendency to previous graphs (3a), where glucose levels start at 900 and fall more slowly with smaller fractional orders. Fig. 3b illustrates a significant increase in insulin levels as a result of the high starting glucose. The amount of time it takes to achieve the insulin peak depends on the fractional order. Fig. 3c exhibits minimal variations, consistently holding values at approximately 300, in line with previous figures has a distinct intial condition that is centered on the number of beta cells. The glucose levels in Fig. 4a decrease at different rates from higher values, which are managed by the fractional orders. The levels of insulin (4b) exhibit notable rises that take longer to reach their peak due to smaller fractional orders. All fractional orders in Fig. 4c remain near 300, showing steady beta-cell numbers. Fig. 5a shows glucose levels with an initial beta-cell count of 600. The decrease pattern is impacted by fractional orders, indicating different rates of decay. Shows significant rises in insulin as seen in Fig. 5b, with smaller fractional orders exhibiting a noticeable delay in peak insulin levels. Remains approximately 600 in Fig. 5c, demonstrating a gradual decline over time that is constant across various fractional orders. Glucose levels are depicted in Fig. 6a starting at 900. Fractional orders affect the rate at which glucose levels decrease. Fig. 6b shows a significant increase in insulin levels, with the fractional order having an effect on the time to peak. The beta-cell in Fig. 6c stabilizes at approximately 900, showing little change over fractional orders. Fig. 7a illustrates the change in G(t) over time, starting from 0. The glucose level increases and then stabilizes. Illustrates (7b) G(t) starting from a higher initial value and stabilizing at a normal level after an initial increase. In Fig. 7c focuses on smaller time intervals and slight variations in G(t) at normal values. In (8a) displays I(t) over time starting from 0. Insulin levels rise and stabilize. In Fig. 8b, I(t) starts from a higher initial value, experiences a significant increase, and then stabilizes. Focuses on a smaller time frame in Fig. 8c, showing fine variations in insulin levels. In (9a), it shows the change in $\beta(t)$ over time, starting from a lower value and increasing slightly. In (9b), it demonstrates $\beta(t)$ starting from a normal value and maintaining

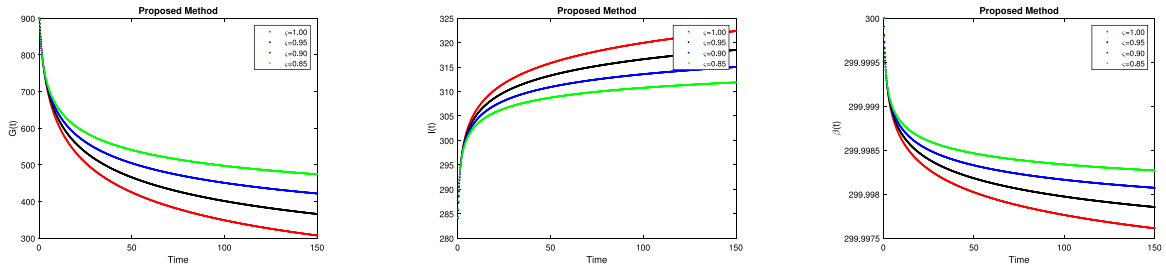

(a) (b) (c)

Fig. 3. Simulation of $G(t), I(t), \beta(t)$ at G = 900.

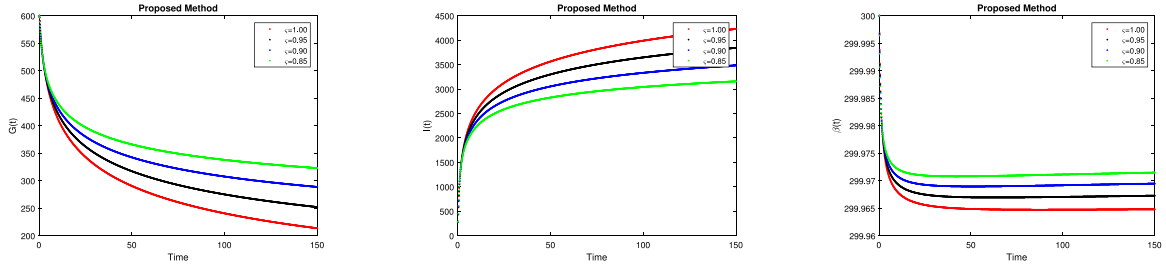

(a) (b) (c)

Fig. 4. Simulation of $G(t), I(t), \beta(t)$ at $\beta = 300$.

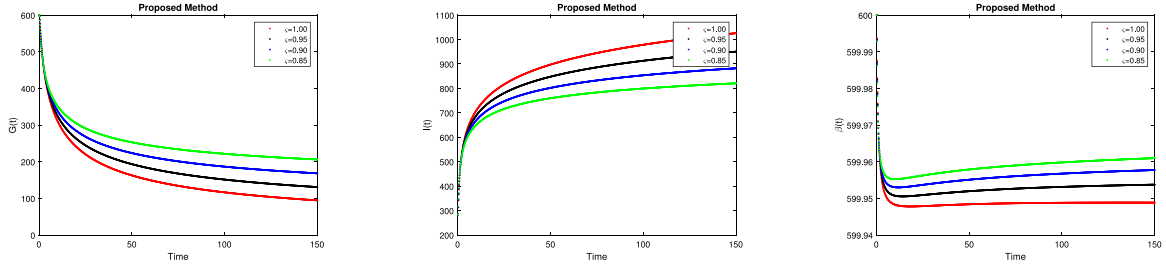

(a) (b) (c)

Fig. 5. Simulation of $G(t), I(t), \beta(t)$ at $\beta = 600$.

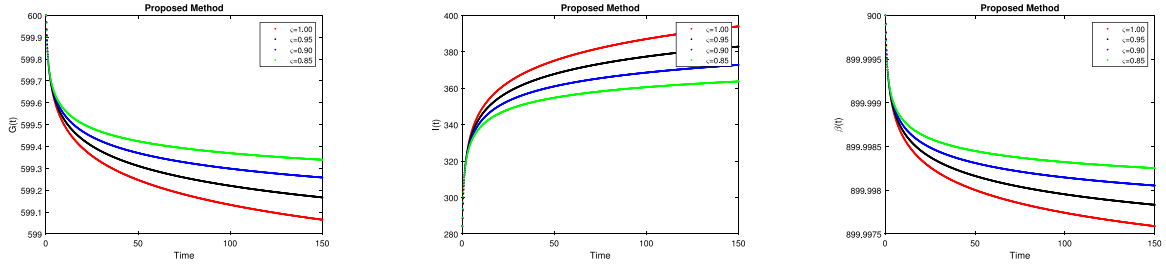

(a) (b) (c)

Fig. 6. Simulation of $G(t), I(t), \beta(t)$ at $\beta = 900$.

stability with minimal fluctuations. It focuses on a very narrow range of beta-cell values, showing slight variations in Fig. 9c. In Fig. 10, the proposed method displays a unique pattern of glucose level stabilization that is different from the Power-Law and Exponential-Decay models. Between the Power-Law model and the suggested approach, the Mittag-Leffler model exhibits behavior that is in between. Across models, the glucose levels fall and stabilize in diverse ways; the suggested approach offers a distinct stabilization pattern from the others. While glucose stabilizes at different rates in different models, the suggested approach produces a unique stabilization curve. In contrast to the Power-Law and Exponential-Decay models, the suggested approach displays a unique pattern when it comes to the rates at which glucose levels stabilize. Compared to the other models, the suggested approach exhibits a distinct pattern of insulin level growth and stabilization in Fig. 11. Different insulin levels rise and stabilize in different ways, and the suggested strategy offers a distinct pattern of stabilization. Insulin levels exhibit different patterns of rise and plateau, and the suggested approach behaves differently from other models. While insulin level changes vary in different models, the suggested approach offers a distinct stability curve. The beta-cell levels in Fig. 12 show

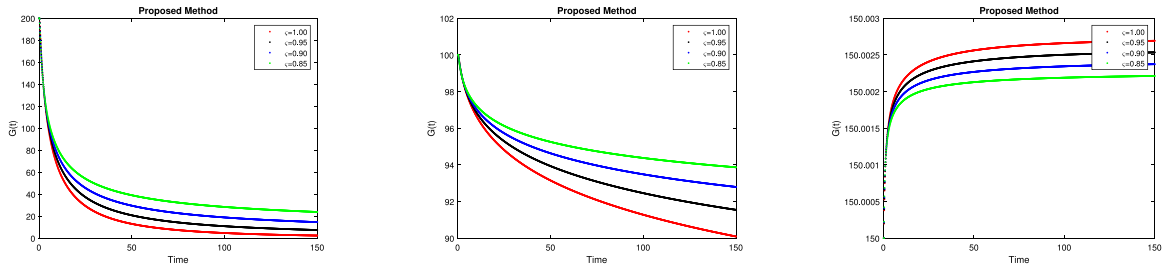

(a) (b) (c)

Fig. 7. Simulation of G at different normal values.

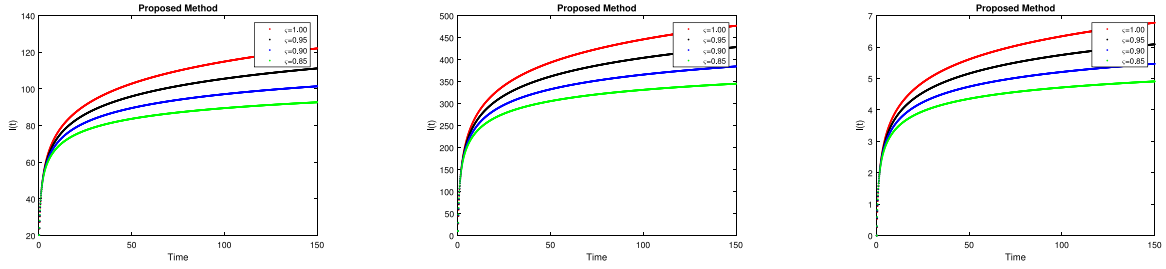

(a) (b) (c)

Fig. 8. Simulation of I at different normal values.

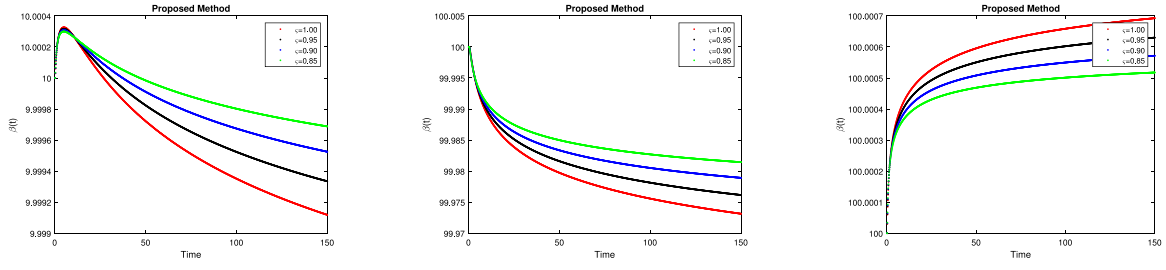

(a) (b) (c)

Fig. 9. Simulation of β at different normal values.

some diversity in patterns of stability, but overall stability is maintained across all models. The suggested approach offers a marginally different stabilizing pattern, while beta-cell levels exhibit negligible alterations. Beta-cell levels change slightly, and the suggested approach has unique stability features. The suggested strategy has a unique signature pattern; however multiple models show a common beta-cell stabilization. The model demonstrates that stress-induced adrenaline release leads to prolonged hyperglycemia, with simulations showing how changes in fractional order values and fractal dimensions affect glucose regulation. For instance, lower fractional order values, indicating higher stress, result in delayed insulin response and slower glucose reduction. These findings highlight the effectiveness of the proposed fractional-order PID controller in adapting to different physiological conditions, ensuring better glucose management during stress, excitement, or trauma.

On the other hand, in our study we are able to capture the dynamics of this diabetes mellitus model because using ABC fractional order derivative. Experiments of simulation reveal that the numerical results might be significantly influenced by slight alteration in derivative order. Accordingly, to achieve high accuracy level in the results with real data accurately determining the value of fractional order becomes necessary. This is a more detailed qualitative analysis of the simulation outcomes obtained using different fractional orders in ς for diabetes mellitus model, that provides new knowledge on the dynamics of this disease. Glucose regulation, insulin sensitivity, oscillatory behavior as well as long term stability and clinical importance are essential aspects allowing for a more complete understanding of the underlying mechanisms and an evaluation of data implications.

Thus, the numerical simulations performed within the context of this study are deliberately constructed to assess the performance of the fractional-order PID controller in various conditions, which may be encountered in reality. These simulations provide a comprehensive look at the performance of the controller under varying initial conditions and parameter values, in situations ranging from normal to those at the extremes of pathophysiological conditions. This approach not only rewards the effective functioning of the controller in maintaining blood glucose levels, but also sheds light on other aspects of its performance in various and particularly conditions. The fact that the present work employs a simulation-based assessment of the model renders the conclusions more robust and increases the practical relevance and efficacy of the proposed model in managing diabetes.

9. Conclusion

The analysis of the mathematical model of diabetes mellitus in this study involves the application of fractional calculus. More specifically, a nonsingular kernel has been incorporated into the model through the use of the fractional ABC derivative. The fractional-order model's physiologically relevant predictions, especially in cases of severe hyperglycemia induced by adrenaline, closely mirror clinical observations

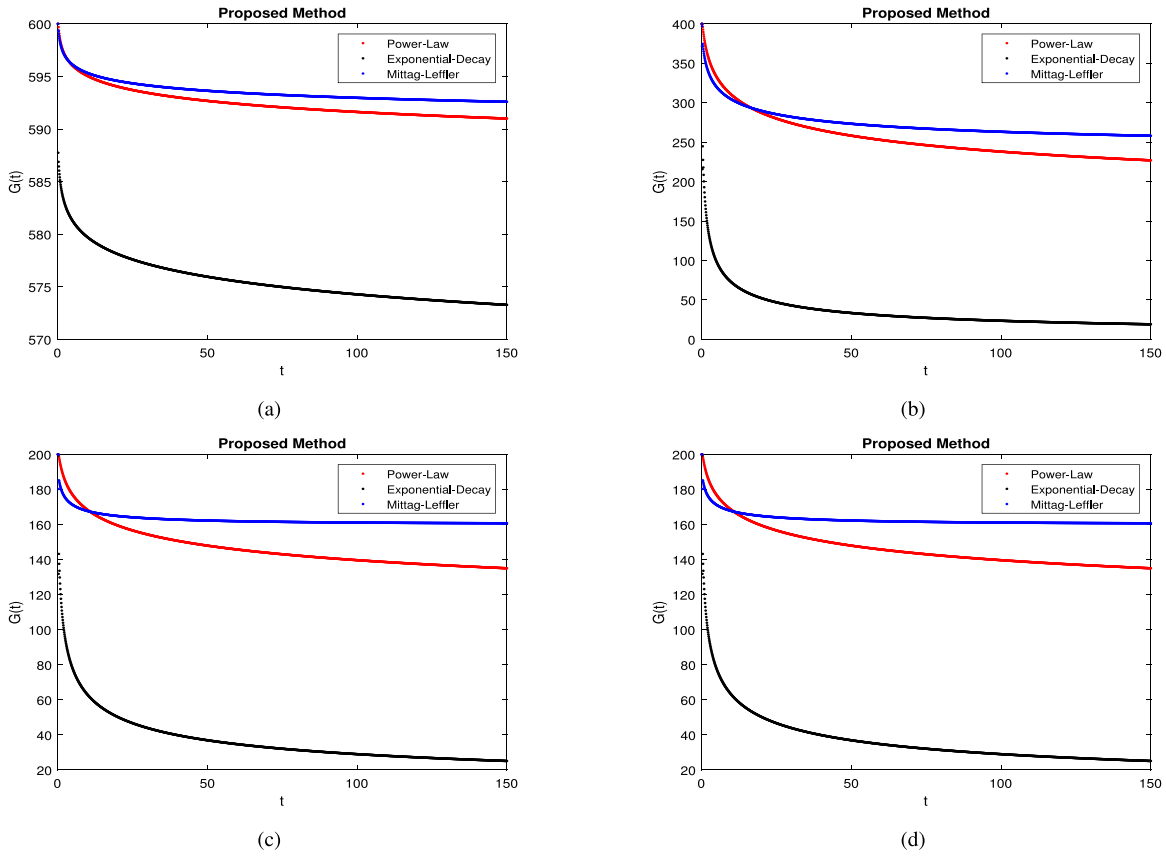

Fig. 10. Comparison of G(t) dynamics at (0.99,0.90,0.85,0.8) respectively with different kernels.

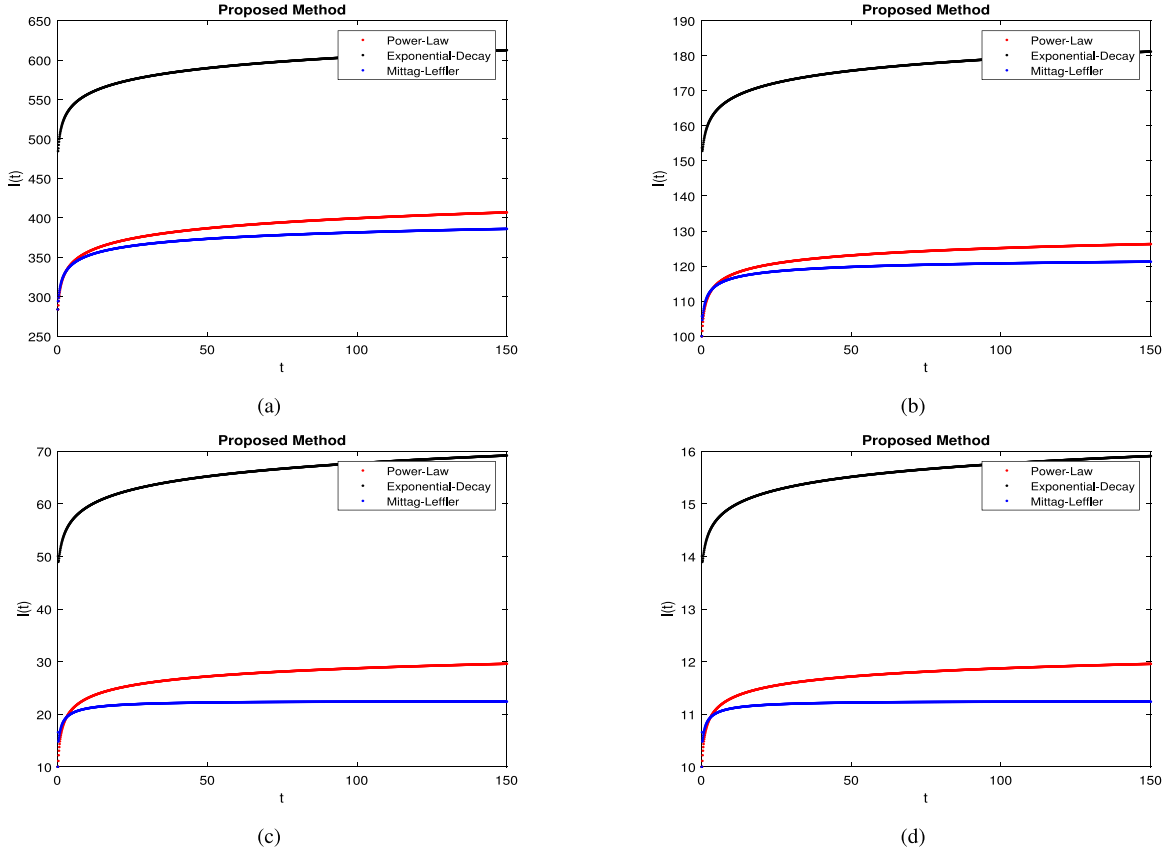

Fig. 11. Comparison of I(t) dynamics at (0.99,0.90,0.85,0.8) respectively with different kernels.

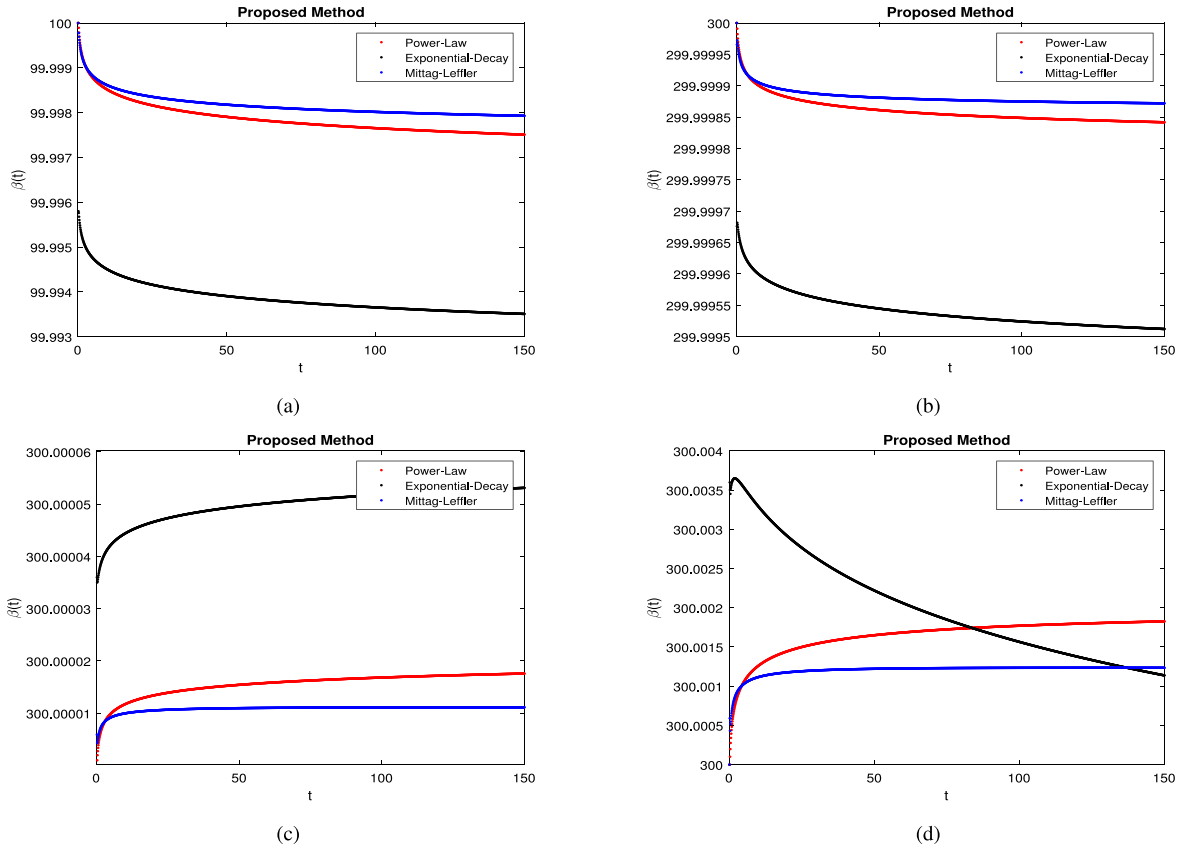

Fig. 12. Comparison of β Cells Mass dynamics at (0.99,0.90,0.85,0.8) respectively with different kernels.

and experimental data, underscoring its validity and potential utility in personalized diabetes management and enhancing our understanding of stress-induced glucose dynamics. An efficient numerical approximation method was created to discretize the proposed model, allowing for computer analysis and practical application. We prove existence and uniqueness of a system of solutions for the modified diabetes mellitus model under certain conditions by applying fixed point theory. Ulam–Hyers stability was investigated in order to evaluate the fractional model's qualitative characteristics, well-posedness, and robustness. PID controllers offer more tuning parameters, which enable more precise management of the dynamics of the system with different initial conditions for normal and diabetes patients. The optimization of fractional orders (ς, χ) in the tuning of the fractional-order PID controller has proven effective for glucose regulation under various conditions. Simulation-based testing further confirms the controller's reliable performance in challenging scenarios, such as stress and trauma, underscoring the system's robustness and suitability for real-world applications. They may withstand external disruptions and adjustments in system settings more resiliently enhanced performance with respect to steady-state error, settling time, and overshoot. The suggested algorithm may be expanded in the future to handle a variety of biological and physical models. The suggested approach can be specifically used to analyze fractional-order models with comparison of other kernels for accuracy and management of proposed techniques. Additionally, the outcome of the numerical experiment showed that prolonged hyperglycemia was caused by frequent production of adrenaline into the blood. We suggest widespread and ongoing health education in light of the study's findings, particularly for communities residing in places where the aforementioned agents of epinephrine secretion trauma, excitement, and stress are prevalent. Employing non-local and non-singular kernel operators, such as Caputo–Fabrizio and Caputo can effectively capture natural phenomena compared to traditional mathematical operators, offering deeper insights into the diabetes mellitus model. These fractional operators are capable of representing the diabetes mellitus disease, and it is important to evaluate their respective advantages and disadvantages. Fractal dimensions in the fractional-order model capture the physiological complexity of glucose–insulin dynamics, crucial for accurate diabetes management. Changes in these dimensions reflect different states, from stable control to chaotic blood sugar levels. Understanding and utilizing these properties can enhance personalized treatment, offer insights into disease progression, and improve diabetes management, particularly under stress or trauma. The organizations, and public health professionals should concentrate on public education initiatives that help members of the public comprehend how these three factors raise their own risk of developing diabetes. Therefore, it would be advantageous for young researchers in this field to compare their findings with the results of this study.

Implementing a fractional-order PID controller in a real-world clinical setting is feasible but comes with several challenges that need to be addressed. The potential benefits of improved performance, stability, and adaptability in managing diabetes make this an attractive option, but practical considerations such as regulatory approval, user training, cost, and system integration must be carefully managed. With the right infrastructure and support, fractional-order PID controllers could significantly enhance diabetes management, offering patients more precise and personalized control over their blood glucose levels. While the fractional-order PID controller model presents significant theoretical benefits for managing insulin–glucose dynamics, addressing its limitations such as the need for greater physiological complexity, the development of adaptive controllers, and extensive clinical validation-will be crucial for advancing the model from a theoretical framework to a practical tool suitable for widespread clinical adoption.

CRediT authorship contribution statement

Kottakkaran Sooppy Nisar: Writing – review & editing, Writing – original draft, Validation, Supervision, Software, Methodology,

Conceptualization. **Muhammad Farman:** Writing – original draft, Visualization, Methodology, Investigation, Conceptualization. **Khadija Jamil:** Writing – original draft, Software, Investigation. **Saba Jamil:** Writing – original draft, Visualization, Software, Investigation. **Evren Hincal:** Writing – original draft, Validation, Formal analysis.

Funding

None

Declaration of competing interest

The author declare that this manuscript is neither published nor submitted in any other journal.

Acknowledgment

"This study is supported via funding from Prince Sattam bin Abdulaziz University, Saudi Arabia project number (PSAU/2024/R/1445)"

References

[1] B. Kwach, O. Ongati, R. Simwa, Mathematical model for detecting diabetes in the blood, 2011.
[2] A.A. Sharief, A. Sheta, Developing a mathematical model to detect diabetes using multigene genetic programming, Int. J. Adv. Res. Artif. Intell. 3 (10) (2014).
[3] B. Topp, K. Promislow, G. Devries, R.M. Miura, D.I.A.N.E. T Finegood, A model of ß-cell mass, insulin, and glucose kinetics: pathways to diabetes, J. Theoret. Biol. 206 (4) (2000) 605–619.
[4] J. Hussain, D. Zadeng, A mathematical model of glucose-insulin interaction, Sci. Vis. 14 (2) (2014) 84–88.
[5] A. Atangana, Mathematical model of survival of fractional calculus, critics and their impact: How singular is our world? Adv. Difference Equ. 2021 (1) (2021) 403.
[6] M. Farman, M.U. Saleem, A. Ahmad, S. Imtiaz, M.F. Tabassum, S. Akram, M.O. Ahmad, A control of glucose level in insulin therapies for the development of artificial pancreas by Atangana Baleanu derivative, Alex. Eng. J. 59 (4) (2020) 2639–2648.
[7] C. Xu, M. Farman, A. Hasan, A. Akgül, M. Zakarya, W. Albalawi, C. Park, Lyapunov stability and wave analysis of Covid-19 omicron variant of real data with fractional operator, Alex. Eng. J. 61 (12) (2022) 11787–11802.
[8] K.S. Nisar, M. Farman, M. Abdel-Aty, C. Ravichandran, A review of fractional order epidemic models for life sciences problems: Past, present and future, Alex. Eng. J. 95 (2024) 283–305.
[9] K.S. Nisar, M. Farman, M. Batool, C. Xu, Mathematical analysis and modeling of fractional order human brain information dynamics including the major effect on sensory memory, Cogent Eng. 11 (1) (2024) 2301161.
[10] S. Jamil, P.A. Naik, M. Farman, M.U. Saleem, A.H. Ganie, Stability and complex dynamical analysis of COVID-19 epidemic model with non-singular kernel of Mittag-Leffler law, J. Appl. Math. Comput. (2024) 1–36.
[11] K.S. Nisar, M. Farman, K. Jamil, A. Akgul, S. Jamil, Computational and stability analysis of Ebola virus epidemic model with piecewise hybrid fractional operator, Plos One 19 (4) (2024) e0298620.
[12] M. Farman, N. Gokbulut, U. Hurdoganoglu, E. Hincal, K. Suer, Fractional order model of MRSA bacterial infection with real data fitting: Computational analysis and modeling, Comput. Biol. Med. 173 (2024) 108367.
[13] A. Atangana, Fractal-fractional differentiation and integration: connecting fractal calculus and fractional calculus to predict complex system, Chaos Solitons Fractals 102 (2017) 396–406.
[14] M. Farman, R. Sarwar, A. Akgul, Modeling and analysis of sustainable approach for dynamics of infections in plant virus with fractal fractional operator, Chaos Solitons Fractals 170 (2023) 113373.
[15] A. Akgül, M. Farman, A. Ahmad, A. Khan, S. Zahran, W.S. Awad, Fractional order glucose insulin model with generalized Mittag-Leffler kernel, Appl. Math. 17 (2) (2023) 365–374.
[16] S. Jamil, M. Farman, A. Akgül, Qualitative and quantitative analysis of a fractal fractional HIV/AIDS model, Alex. Eng. J. 76 (2023) 167–177.
[17] K. Sadri, K. Hosseini, E. Hinçal, D. Baleanu, S. Salahshour, A pseudo-operational collocation method for variable-order time-space fractional KdV-Burgers-Kuramoto equation, Math. Methods Appl. Sci. (2023).
[18] M. Farman, M. Batool, K.S. Nisar, A.S. Ghaffari, A. Ahmad, Controllability and analysis of sustainable approach for cancer treatment with chemotherapy by using the fractional operator, Results Phys. (2023) 106630.
[19] A. Omame, F.D. Zaman, Analytic solution of a fractional order mathematical model for tumour with polyclonality and cell mutation, Partial Differ. Equ. Appl. Math. 8 (2023) 100545.
[20] A. Omame, I.P. Onyenegecha, A.A. Raezah, F.A. Rihan, Co-dynamics of covid-19 and viral hepatitis b using a mathematical model of non-integer order: impact of vaccination, Fractal Fract. 7 (7) (2023) 544.
[21] C.O. Agwu, A. Omame, S.C. Inyama, Analysis of mathematical model of diabetes and tuberculosis co-infection, Int. J. Appl. Comput. Math. 9 (3) (2023) 36.
[22] N. Sene, Numerical methods applied to a class of SEIR epidemic models described by the Caputo derivative, in: Methods of Mathematical Modeling, Academic Press, 2022, pp. 23–40.
[23] N. Sene, A. Ndiaye, Existence and uniqueness study for partial neutral functional fractional differential equation under Caputo derivative, Int. J. Optim. Control: Theor. Appl. (IJOCTA) 14 (3) (2024) 208–219.
[24] A. Khan, A.U.K. Niazi, S. Rehman, S. Ahmed, Hostile-based bipartite containment control of nonlinear fractional multi-agent systems with input delays: a signed graph approach under disturbance and switching networks, AIMS Math. 9 (5) (2024) 12678–12699.
[25] A. Khan, A.U.K. Niazi, W. Abbasi, F. Awan, M.M.A. Khan, F. Imtiaz, Cyber secure consensus of fractional order multi-agent systems with distributed delays: Defense strategy against denial-of-service attacks, Ain Shams Eng. J. 15 (4) (2024) 102609.
[26] A. Khan, A.U.K. Niazi, H. Raza, W. Abbasi, F. Awan, Resilient based consensus of fractional-order delayed multi-agent systems in Riemann–Liouville sense, Alex. Eng. J. 80 (2023) 348–357.
[27] A. Khan, W.U. Hassan, A. Manzor, S. Ahmed, A.U.K. Niazi, Strengthening stability with centralized event-triggered control system with the disturbances and artificial time delay in wireless connected vehicle platooning (CVSs), Syst. Sci. Control Eng. 12 (1) (2024) 2342818.
[28] M. Farman, M. Amin, A. Akgül, A. Ahmad, M.B. Riaz, S. Ahmad, Fractal-fractional operator for COVID-19 (Omicron) variant outbreak with analysis and modeling, Results Phys. 39 (2022) 105630.
[29] A. Atangana, Mathematical model of survival of fractional calculus, critics and their impact: How singular is our world? Adv. Difference Equ. 2021 (1) (2021) 1–59.
[30] G.M. Nchama, L.L. Alfonso, A.L. Mecías, M.R. Ricard, Properties of the Caputo–Fabrizio fractional derivative, Int. J. Appl. Eng. Res. 16 (1) (2021) 13–21.
[31] I.I. Mohammed, I.I. Adamu, S.J. Barka, Mathematical model for the dynamics of glucose, insulin and ß-cell mass under the effect of trauma, excitement and stress, Model. Numer. Simul. Mater. Sci. 9 (04) (2019) 71.